Loss of hepatic aldolase B activates Akt and promotes hepatocellular carcinogenesis by destabilizing Aldob/Akt/PP2A protein complex

Xuxiao He[1,2,7], Min Li[1,2,7], Hongming Yu[4], Guijun Liu[1,2], Ningning Wang[1,2], Chunzhao Yin[2,3], Qiaochu Tu[2,3], Goutham Narla[6], Yongzhen Tao[1*], Shuqun Cheng[4*] and Huiyong Yin[1-3,5,8*]

[1]CAS Key Laboratory of Nutrition, Metabolism and Food Safety, Shanghai Institute of Nutrition and Health, Chinese Academy of Sciences (CAS), Shanghai, China 200031

[2]University of the Chinese Academy of Sciences, CAS, Beijing, China 100049

[3]School of Life Science and Technology, ShanghaiTech University, Shanghai, China 201210

[4]The Eastern Hepatobiliary Surgery Hospital, Shanghai, China 200433

[5]Key Laboratory of Food Safety Risk Assessment, Ministry of Health, Beijing, China

[6]Division of Genetic Medicine, Department of International Medicine, University of Michigan, Ann Arbor, Michigan, USA

[7]These two authors contributed equally to this work

[8]Lead Contact

[*]Correspondence: yztao01@sibs.ac.cn, chengshuqun@aliyun.com, or hyyin@sibs.ac.cn

Abstract

Loss of hepatic fructose-1, 6-bisphosphate aldolase B (Aldob) leads to a paradoxical upregulation of glucose metabolism to favor hepatocellular carcinogenesis but the upstream signaling events remain poorly defined. Akt is highly activated in HCC and targeting Akt is being explored as a potential therapy for HCC. Herein we demonstrate that Aldob suppresses Akt activity through a protein complex containing Aldob, Akt, and protein phosphatase 2A (PP2A), leading to inhibition of cell viability, cell cycle progression, glucose metabolism and tumor growth. Interestingly, Aldob directly interacts with phosphorylated Akt (p-Akt) and promotes the recruitment of PP2A to dephosphorylate p-Akt, and this scaffolding effect of Aldob is independent of its enzymatic activity. Loss of Aldob or disruption of Aldob/Akt interaction in Aldob R304A mutant restores Akt activity and tumor promoting effects. Consistently, Aldob and p-Akt expression are inversely correlated in human HCC tissues, and Aldob downregulation coupled with p-Akt upregulation predicts a poor prognosis for HCC. We have further discovered that a specific small-molecule activator of PP2A (SMAP) efficiently attenuates HCC tumorigenesis in Aldob-deficient cell lines and xenografts. Our work reveals a novel non-glycolytic role of Aldob in negative regulation of Akt activation, suggesting that inhibiting Akt activity and reactivating PP2A may be a potential therapeutic approach for HCC treatment.

Introduction

Hepatocellular carcinoma (HCC) is the most common primary liver malignancy and the 4th leading cause of cancer-related deaths worldwide [1]. Despite considerable improvement in the diagnosis and treatment for HCC, the clinical prognosis of HCC remains disappointing primarily as a result of an incomplete understanding of the molecular mechanisms underlying HCC progression and limited therapeutic options [2].

Abnormal activation of the PI3K/Akt signaling pathway is a hallmark of many human malignancies, especially HCC [3]. In response to growth factors or cytokines, activated PI3K generates phosphatidylinositol-3, 4, 5-trisphosphate (PIP_3), which recruits Akt for phosphorylation at threonine 308 (T308) by phosphoinositide-dependent kinase 1 (PDK1) and serine 473 (S473) by mechanistic target of rapamycin complex 2 (mTORC2) [4]. Activated Akt triggers the subsequent cellular response through the phosphorylation of various downstream substrates or induction of multiple gene expression. For instance, inhibitory phosphorylation of glycogen synthase kinase 3β (GSK3β) by active Akt leads to increased stability and accumulation of CyclinD1, thereby promoting cell cycle progression [5]. Besides, activated Akt enhances the expression and activity of numerous glycolytic enzymes, such as glucose transporter, hexokinase 1 (HK1), and phosphofructokinase 1, resulting in the upregulation of glucose uptake and glycolysis [6, 7]. Importantly, a series of feedback controls counteract Akt activation to maintain the transient signal. In addition to signal termination by phosphatase and tensin homolog (PTEN), protein phosphatase 2A (PP2A) and PH domain and leucine rich repeat protein phosphatase (PHLPP) function as Akt phosphatases directly dephosphorylating Akt [8, 9]. Therefore, a delicate

balance between protein kinase-catalyzed phosphorylation and protein phosphatase-mediated dephosphorylation is vital for Akt kinase activity in cellular homeostasis; dysregulation of this balance may lead to tumorigenesis. However, the upstream signaling networks involved in the regulation of Akt activity remain to be fully characterized.

Fructose-1, 6-bisphosphate aldolase catalyzes the cleavage of fructose-1, 6-bisphosphate (FBP) to glyceraldehyde-3-phosphate and dihydroxyacetone phosphate in glycolysis. Aldolase B (Aldob) is abundantly expressed in the liver, kidney and small intestine, whereas aldolase A (Aldoa) and aldolase C (Aldoc) are the muscle isoform and central nervous system isoform, respectively [10]. In humans, gene dysfunction or deficiency of Aldob causes hereditary fructose intolerance (HFI), a recessively inherited disorder of fructose metabolism [11]. Aldolase has been implicated in diverse physiological and pathological processes [12]. A recent study has identified that aldolase acts as a sensor of FBP and glucose availability in the regulation of AMP-activated protein kinase (AMPK) [13]. Dissociation of aldolase from the actin cytoskeleton leads to increased aldolase activity and enhanced glycolytic flux, which is positively regulated by PI3K signaling [14]. Aldob has been documented to be downregulated in HCC tissues in transcriptomic and proteomic studies, which is correlated with multiple malignant characteristics of HCC [15-17]. Our recent study identified a novel tumor-suppressive mechanism by which Aldob regulates metabolic reprogramming in HCC by interacting with the rate-limiting enzyme in pentose phosphate pathway, glucose-6-phosphate dehydrogenase (G6PD). Loss of Aldob leads

to a novel mode of metabolic reprogramming in favor of glucose metabolism by upregulating glycolysis, PPP and TCA for HCC progression. However, the upstream signaling events leading to HCC progression and metabolic reprogramming due to the loss of Aldob remain largely unknown.

Here we report that Aldob negatively regulates Akt activation, which is required for Aldob-induced suppression of cancer cell proliferation, glucose metabolism and tumorigenesis. Aldob directly binds to p-Akt potentiating PP2A interaction and dephosphorylation of p-Akt, resulting in the inhibition of Akt phosphorylation and downstream oncogenic signaling. This novel protein interaction appears to be independent of Aldob enzymatic activity. Moreover, a novel small molecule activator of PP2A (SMAP) elicits anti-tumor efficacy comparable to Akt allosteric inhibitor (MK2206) in blocking the tumorigenic effects driven by Aldob deficiency *in vitro* and *in vivo*. Interestingly, we discover an inverse correlation between Aldob and p-Akt expression in HCC tumor tissues, and a combination of low Aldob and high p-Akt expression is associated with the worst prognosis for HCC patients. Collectively, our work highlights that targeting Akt is a viable approach to treat HCC and PP2A activation using small molecule modulators of this phosphatase has the potential as a new targeted approach for HCC treatment.

Results

Aldob expression is negatively correlated with Akt activation in human HCC and the expression of Aldob/p-Akt predicts overall survival of HCC patients

Our recent study has revealed a novel tumor suppressive role for the glycolytic enzyme Aldob in HCC through directly binding to G6PD and inhibiting its activity, acting as a metabolic switch in glucose metabolism and regulating the metabolic reprogramming. Accumulating body of evidence has demonstrated that metabolic reprogramming in cancer cells to meet increased bioenergetic and biosynthetic requirements during tumorigenesis depends on multiple intracellular signaling pathways [18]. Among them, activated Akt signaling has a profound impact on metabolic reprogramming through upregulating glycolytic enzymes and promoting aerobic glycolysis [19]. Therefore, we set out to examine the role of Akt signaling in HCC in the context of Aldob downregulation and metabolic reprogramming. We first investigated the clinical relevance between Aldob expression and Akt activation in human HCC. As showed in Fig 1A, reduced Aldob expression and enhanced Akt phosphorylation levels at both the threonine 308 (pT308-Akt) and serine 473 (pS473-Akt) residues were observed in tumor tissues as compared to matched adjacent normal liver tissues. Next, we performed tissue microarray (TMA) analysis in paired clinical samples from HCC patients (Fig 1B; S1 Table, n=70). Aldob expression was negatively correlated with Akt activation in human HCC tissues (Fig 1C, R^2=0.146, p=0.001). We also found that low Aldob expression was significantly correlated with α-fetoprotein (AFP), albumin level, and tumor encapsulation (S1 Table). Kaplan-Meier survival analysis showed that the overall survival time for patients with low Aldob expression was notably shorter than those with high Aldob expression (Fig 1D, p=0.016). Conversely, patients with high pT308-Akt level exhibited shorter overall survival

compared with patients with low pT308-Akt level (Fig 1E, p=0.029). In addition, an elevated level of p-Akt was significantly correlated with prothrombin time, number of tumors, and tumor encapsulation (S1 Table). More importantly, a low Aldob expression coupled with high pT308-Akt levels was associated with the worst overall prognosis (Fig 1F, p=0.001). In conclusion, our study uncovers a novel inverse correlation between Aldob and p-Akt expression in human HCC and low Aldob expression with high p-Akt predicts the worst prognosis for HCC patients, suggesting an important role of Akt signaling in HCC in the context of Aldob downregulation.

Aldob inhibits Akt kinase activity and downstream signaling in HCC

To investigate the relationship of Aldob downregulation and activation of Akt signaling, we observed that, in liver-specific *ALDOB* knockout (KO) mouse primary hepatocytes (PHs), Aldob deletion significantly augmented Akt activation compared to wild-type (WT) PHs, as evidenced by increased levels of pT308-Akt, pS473-Akt and Akt downstream targets, including pS9-GSK3β and pT389-S6K, without affecting the expression of Akt, GSK3β, and S6K (Fig 2A). Notably, we also detected a significantly enhanced expression of HK1, a key enzyme in the first irreversible step of glycolysis by catalyzing the ATP-dependent phosphorylation of glucose to glucose-6-phosphate, which plays a critical role in cellular glucose uptake and utilization [20], suggesting that loss of Aldob may facilitate glucose metabolism through activation of Akt signaling (Fig 2A). Similarly, we observed a prominent elevation of Akt kinase activity in liver tissues of *ALDOB* KO mice compared to WT mice after diethylnitrosamine

(DEN) treatment (Fig 2B). These data suggest a potential tumor-suppressive role of Aldob through inhibiting oncogenic Akt activity, consistent with our previous work that loss of Aldob promotes DEN-induced HCC tumorigenesis in *ALDOB* KO mice.

To further address the role of Aldob in the regulation of Akt phosphorylation in HCC, we generated stable Aldob-overexpressing liver cancer cell lines Huh7 and LM3, which at baseline express low levels of Aldob, and found that ectopic expression of Aldob resulted in a marked reduction of Akt, GSK3β and S6K phosphorylation levels (Fig 2C). Conversely, silencing Aldob by siRNA restored Akt phosphorylation and its downstream targets (Fig 2D). Next, we analyzed the kinetics of Akt activation and attenuation in response to insulin (Fig 2E) and epidermal growth factor (EGF) (Fig 2F) stimulation. Downregulation of Aldob led to increased levels of pT308-Akt, pS473-Akt with coordinate changes in immediate Akt downstream substrate pS9-GSK3β expression in a time-dependent manner (Fig 2E and 2F). Additionally, we performed an *in vitro* Akt kinase assay and demonstrated that overexpressed Aldob dramatically inhibited Akt kinase activity, as assessed by the decreased phosphorylation level of Akt substrate GSK3α (Fig 2G). Taken together, all these results strongly suggest that Aldob suppresses Akt phosphorylation and its kinase activity in HCC.

Aldob inhibits Akt kinase activity and suppresses HCC through impeding cell cycle progression and attenuating glycolysis and TCA metabolism

Given that aberrant activation of Akt signaling promotes cancer progression through regulating cell proliferation, metabolism and survival [3], we next investigated the

functional consequence of Aldob-mediated suppression of Akt kinase activity. We observed that enforced expression of Aldob inhibited cell viability and colony formation capability. Consistently, inhibition of Akt activity by MK2206, a highly selective allosteric Akt inhibitor [21], significantly blocked cell proliferation and eliminated the growth inhibitory effects of Aldob expression (Fig 3A and B). Furthermore, activation of Akt signaling by ectopic expression of Myc-Akt1 significantly enhanced cell survival and abolished Aldob overexpression-induced cell growth arrest (S1A and S1B Fig). These results indicate that Akt-dependent signaling plays an essential role in Aldob-mediated suppression of HCC cell proliferation. Meanwhile, Aldob overexpression or inhibiting Akt activity by MK2206 significantly increased the proportion of cells in the G1-phase, resulting in a decreased percentage of cells in S-phase, indicating that Aldob induces cell cycle arrest at the G1-to-S transition (Fig 3C). Consistent with this observation, up-regulated Aldob or Akt inhibition by MK2206 obviously reduced pT308-Akt, pS473-Akt, pS9-GSK3β and CyclinD1 expression, while elevating the levels of cell cycle inhibitors p21 and p27 (Fig 3D). More importantly, alteration of Akt activation dramatically diminished the effects of Aldob on cell cycle progression and cell cycle-related proteins expression (Fig 3C and D; S1C and S1D Fig).

Metabolic reprogramming has been recognized as the core hallmark for various cancers [22]. Enhanced aerobic glycolysis, known as the Warburg effect, is frequently observed along with abnormally high rates of glucose uptake in rapidly proliferating cancer cells [23]. As the central route of oxidative phosphorylation, the tricarboxylic

acid (TCA) cycle is also upregulated to meet increased cellular energy, biosynthesis and redox needs [24, 25]. The downstream effectors of Akt signaling play a central role in cancer cell metabolic reprogramming. To further determine whether Aldob-mediated inhibition of Akt activity is involved in Aldob-induced metabolic reprogramming, we used stable isotope labeled [U-$^{13}C_6$] glucose as a tracer to track intracellular metabolic flux (Fig 3E). The M+3 (^{13}C labeled at all three positions) fraction of enriched labeled metabolites in glycolysis including pyruvate, lactate and alanine were significantly decreased in Huh7-Aldob cells compared with control (Fig 3F). Meanwhile, Aldob overexpression also observably reduced the M+2 (^{13}C labeled at two positions) fraction of labeled metabolites in TCA cycle, such as fumarate, malate, aspartate, glutamate and citrate (Fig 3G). Besides, blocking Akt activity by MK2206 efficiently weakening Aldob-induced inhibition of metabolic flux in glycolysis and TCA cycle (Fig 3F and G). These results suggest that Aldob suppresses Akt activity, resulting in decreased cellular metabolism in glycolysis and TCA.

On the other hand, knockdown of Aldob via siRNA markedly enhanced Akt activity, promoted cell proliferation and cell cycle progression, increased the fraction of M+3 labeled metabolites from U-^{13}C-glucose in glycolysis and of M+2 labeled metabolites in TCA cycle, and rescued overexpressed Aldob-mediated inhibition of cell growth and metabolism (S2A-H Fig). Moreover, MK2206 exposure also reversed the growth-promoting effects of Aldob knockdown in Huh7-Aldob cells (S2A-H Fig). We found similar patterns of cell proliferation and cell cycle progression effects in LM3 cells (S3A-D Fig). These results suggest that Aldob impedes cell cycle progression and

represses glucose metabolism through inhibiting Akt signaling, which contributes to Aldob-induced cell growth suppression.

We then established a subcutaneous xenograft mouse model to investigate the effects of Aldob expression on tumorigenesis *in vivo*. As illustrated in Fig 3H-I, tumors derived from Huh7-Aldob cells exhibited slower growth and smaller sizes than those from Huh7-Vector cells. Inhibition of Akt activity by MK2206 alone significantly inhibited tumor growth. Additionally, a combination of Aldob overexpression and inhibition of Akt activity showed additive effect on tumor growth inhibition. Interestingly, Huh7-Vector cells appeared to be more responsive to MK2206 than Huh7-Aldob cells in which Akt signaling was already suppressed at baseline. Moreover, Ki67 expression was consistent with the differences noted in tumor weights and size (S1E Fig). Likewise, western blot analysis revealed that Aldob overexpression and MK2206 treatment alone significantly inhibited Akt activation and its downstream signaling compared to control group, respectively, and the combination of the two had the lowest levels of Akt signaling-related proteins (S1F Fig). No changes in body weight were observed throughout the study (S1G Fig). Together, these data demonstrate that Aldob exhibits tumor suppressive effects through inhibition of Akt signaling *in vitro* and *in vivo*; inhibition of Akt activity by the allosteric inhibitor suppresses tumorigenesis caused by the loss of Aldob.

Aldob directly interacts with Akt to suppress Akt activity and HCC cell growth, whereas disruption of Aldob/Akt interaction in Aldob mutant cells restores Akt

activity and cell proliferation

Next, we tested whether Aldob modulated Akt activity through a protein-protein interaction by performing immunoprecipitation (IP) experiments. As shown in Fig 4A, endogenous Aldob pulled down Akt1 in WT mice liver tissues. Reciprocally, Aldob was detected in the endogenous Akt1 immunocomplex. However, *ALDOB* KO significantly weakened immunoprecipitated interacting proteins, suggesting that Aldob and Akt1 bind with each other. Consistently, the interactions between overexpressed Aldob and endogenous or exogenous Akt1 were observed by co-IP assays in HCC cell lines (Fig 4B and C; S3E Fig). Knockdown of Aldob or Akt1 expression by siRNA greatly decreased Aldob interaction with Akt1 (Fig 4B). Moreover, we detected a direct interaction between the recombinant GST-Akt1 and His-Aldob performed by GST pull-down analysis (Fig 4D). In addition, Aldob and Akt2 combined with each other (S4A Fig). Collectively, these results demonstrate that Aldob physically interacts with Akt.

Hepatic Aldob is indispensable for glucose and fructose metabolism, and its deficiency as result of *ALDOB* gene mutation leads to HFI in humans [26]. The residues at Arg43, Arg46, Lys108, Lys147, Arg149, Lys 230 and Arg304 line within the active site pocket of Aldob, and play an important role in substrate binding and catalysis [27, 28]. Mutations involved in aforementioned residues have been identified in the *ALDOB* gene of HFI patients [29, 30]. To determine whether the enzymatic activity of Aldob is required for the this novel interaction, we individually mutated the seven positively charged amino acid residues to alanine and found that among the four point mutants (R43A, K108A, K230A, and R304A) with considerably reduced Aldob-Akt interaction,

they exhibited varied Aldob enzymatic activities: R43A and K230A (completely dead), K108A (32.1%) and R304A (49.1%) of WT Aldob (Fig 4E). Among them, R304A mutant has the most significantly attenuated interactions with Akt. Moreover, the other three mutants (R46A, K147A, and R149A) with moderately attenuated Aldob-Akt interaction, also had variable enzyme activities: R46A maintained 60.2% activity and the other two did not have significant enzyme activity (Fig 4E). Together, these data clearly indicate that the interaction of Aldob with Akt is independent of Aldob enzymatic activity.

To further identify the Akt interacting region on Aldob, a full-length and two truncated mutants of Aldob including a.a. 1-155 (amino acid 1-155 fragment containing clone), and a.a. 1-240 were constructed to examine their Akt-binding capability. Intriguingly, both Aldob truncated mutants failed to interact with Akt compared to the full-length Aldob, indicating that the C-terminal region of Aldob (a.a. 241-364) is most likely the region for Akt interaction (S4B Fig), consistent with the observation that R304A has the weakest Aldob-Akt interaction. We next tested whether Aldob-Akt interaction is essential for Aldob regulation of Akt activity and HCC cell growth. Overexpression of WT Aldob significantly downregulated Akt signaling, whereas disruption of Akt/Aldob interaction in R304A mutant abrogated Aldob-induced inhibition of Akt signaling (Fig 4F). Consistently, R304A mutant efficiently rescued cell viability, colony formation, and cell cycle progression in Aldob-overexpressing cells (Fig 4G-I). Together, these data indicate that Aldob directly interacts with Akt to suppress Akt activity and disruption of this interaction releases Akt kinase activity to

promote cancer cell growth.

Aldob preferentially associates with Akt in a phosphorylation-dependent manner

Because the state of Akt phosphorylation is critical for the integration of various extracellular cues to downstream signaling events for multiple biological processes, we next studied whether the phosphorylation state of Akt played any role in the regulation of the protein-protein interaction between Akt and Aldob. To this end, we examined the effect of Akt1 phospho-deficient mutants (Akt1-T308A and Akt1-S473A) on Aldob-binding capability. Compared with Akt1-WT, both Akt1 phospho-deficient mutants displayed reduced binding with Aldob, suggesting that Akt1 kinase activity is critical for Akt1 and Aldob interaction (Fig 5A). Next, we treated Aldob and Akt1 transfected Huh7 cells with insulin or EGF to further examine the correlation between Akt1 phosphorylation status and Aldob interaction with Akt1. Interestingly, the interaction of Aldob and Akt1 tracked with the kinetics of Akt1 activation and attenuation in response to either insulin or EGF, with the binding between Aldob and Akt1 almost peaking when the levels of phosphorylated Akt (p-Akt) were the highest (Fig 5B and C). Furthermore, blocking Akt phosphorylation through MK2206 treatment prominently decreased Aldob interaction with Akt1 (Fig 5D). Together, these results indicate that Aldob preferentially binds to the phosphorylated form of Akt.

Aldob promotes Akt interaction with PP2A and accelerates PP2A-mediated Akt dephosphorylation

Given that Akt interacted with Aldob in an Akt phosphorylation-dependent manner, we hypothesized that phosphatases of Akt may be involved in Aldob-induced repression of Akt activity. Interestingly, as shown in Fig 2, Akt phosphorylation at both T308 and S473 was significantly reduced in response to Aldob expression. Previous study suggested that PP2A directly dephosphorylates Akt at both T308 and S473 [31, 32]. Moreover, phosphorylation of Akt at T308 has been identified to play a more crucial role in activating Akt [33, 34]. Thus we examined the possible involvement of the serine/threonine phosphatase PP2A in Aldob-mediated regulation of Akt activity. Strikingly, we observed an abundance of the catalytic subunit of PP2A (PP2AC), but little PHLPP, in the exogenous Aldob immunocomplex (Fig 6A). Meanwhile, no interaction of Aldob with the Akt kinase PDK1 was observed (Fig 6B).

Since PP2A has been shown to bind directly to Akt and dephosphorylate Akt [35], we speculated that Aldob might nucleate the Akt interaction with PP2A to trigger Akt dephosphorylation resulting in inhibition of downstream signaling. To support this hypothesis, we performed GST pull down assay and found that WT Aldob but not the Akt1-binding deficient Aldob-R304A mutant significantly enhanced Akt1 interaction with PP2AC (Fig 6C). Similarly, endogenous Akt1 pulled down both Aldob and PP2AC in the liver tissue of WT mice, whereas loss of Aldob drastically diminished Akt1-immunoprecipitated Aldob and PP2AC in *ALDOB* KO mice (Fig 4A), further suggesting that Aldob acts as a scaffold protein for the Akt/PP2A complex. Next, we performed *in vitro* PP2A phosphatase activity assay using phosphorylated Akt as a substrate and observed a time-dependent decrease of p-Akt at both T308 and S473

residues upon incubation with active PP2A. More importantly, WT Aldob remarkably augmented the PP2A-induced reduction of p-Akt expression, while no significant effect was found on the Akt1-binding deficient Aldob-R304A mutant (Fig 6D). Furthermore, we examined the effect of okadaic acid (OA) on these processes. OA is an inhibitor of serine/threonine protein phosphatase PP1 and PP2A, exhibiting greater selectivity toward the latter up to concentration of 100 nM [36]. As shown in Fig 6E, OA treatment effectively restored Akt phosphorylation levels in Aldob-overexpressing cells, which almost comparable to untreated control cells, suggesting that Aldob-induced inhibition of Akt activity is dependent on PP2A. To further verify these results in human HCC samples, we randomly selected two pairs of HCC tissue samples for IP assays. The endogenous interaction between Aldob and Akt1 was identified in peripheral normal liver tissues of HCC patients (Fig 6F). However, downregulated Aldob in tumor tissues significantly decreased Akt1-immunoprecipitated Aldob and PP2AC when compared to corresponding adjacent normal tissues (Fig 6F), further suggesting that Aldob/Akt/PP2A signaling is involved in human HCC progression. Taken together, Aldob interacts with p-Akt to promote the recruitment of the phosphatase PP2A and accelerate PP2A-mediated dephosphorylation, which is primarily responsible for Aldob-induced downregulation of Akt phosphorylation.

PP2A activation using SMAP downregulates Akt activity and suppresses HCC progression

PP2A is generally considered as a tumor suppressor that dephosphorylates multiple

critical oncogenic proteins, such as Akt, ERK, and MYC [37]. Functional inactivation of PP2A has been linked to tumor development in many cancers [38]. Thus, pharmacologic restoration of PP2A phosphatase activity has emerged as an attractive strategy for cancer therapy [39]. Recent studies have reported that a series of specific small-molecule activators of PP2A (SMAPs) reengineered from tricyclic neuroleptics effectively activate PP2A, resulting in the dephosphorylation of key targets Akt and ERK, and blocking tumor growth of lung, prostate cancer and pancreatic neuroendocrine tumors both *in vitro and in vivo* [40-43]. The validation of their target specificity, mechanism of action, and pharmaceutic properties have been extensively documented [40-43]. Here we treated Huh7 and LM3 cells with increasing concentrations of SMAP. SMAP-induced PP2A activation was demonstrated by parallel reduction of Akt, ERK and GSK3β phosphorylation levels which was accompanied by decreased CyclinD1 expression (S5A Fig). Moreover, SMAP treatment reduced cell viability in both cell lines in a dose-dependent manner with IC_{50} of approximately 9 μM (Huh7) and 12 μM (LM3), which were similar to those reported in other tumor cell types (S5B Fig). SMAP treatment induced visible HCC cell death. These results indicate that PP2A activation with SMAP results in growth inhibition and cell death in HCC cell lines.

To evaluate the utility of PP2A activation toward Aldob-mediated suppression of Akt activity, Huh7-Vector and Huh7-Aldob cells were treated with 10 μM SMAP for further functional studies. We found that Aldob overexpression and SMAP treatment alone both inhibited cell proliferation, and the combination of the two showed an additive

effect on repressing cell proliferation, as measured by cell viability and clonogenic assays (Fig 7A and B). Additionally, cell cycle analysis revealed that SMAP treatment resulted in a significant increase in the G1 phase with a coordinate loss of the S population, and exacerbated Aldob-induced G1-to-S phase cell cycle arrest (Fig 7C). Western blot analysis showed Aldob overexpression had no effect on ERK phosphorylation in the presence of either DMSO or SMAP, whereas Aldob-induced downregulation of Akt/GSK3β/CyclinD1 signaling was potentiated by SMAP-mediated PP2A activation (Fig 7D). Notably, relative to Huh7-Aldob cells that contain diminished Akt activity, Huh7-Vector cells were more sensitive to SMAP treatment. Together, these results indicate that PP2A plays an essential role in Aldob-induced growth inhibition, and that small molecule mediated PP2A activation is beneficial to Aldob-mediated suppression of Akt signaling and HCC cell growth.

We further investigated the efficacy of SMAP on HCC tumor progression *in vivo*. SMAP treatment alone resulted in dramatic inhibition of tumor growth, which is similar to Aldob overexpression-induced growth-inhibitory effects (Fig 7E-G). There was a moderate reduction in tumor burden of Huh7-Aldob tumors compared with Huh7-Vector tumors with SMAP treatment (Fig 7E-G). It is noteworthy that there was no significant weight loss or behavioral abnormalities during the 3-week treatment, suggesting that SMAP is well-tolerated in this mouse model (S5C Fig). In addition, western blot analysis in SMAP-treated tumors detected the simultaneous decrease in Akt/GSK3β/CyclinD1 signaling and ERK phosphorylation levels, suggesting that SMAP induces PP2A-dependent inhibition of these signaling pathways resulting in

suppression of tumor growth (S5D Fig). IHC analysis validated lower protein levels of Ki67 in SMAP-treated tumors compared with control vehicle-treated tumors (S5E Fig). More importantly, upregulated Aldob-induced attenuation of Akt signaling and tumor growth was greatly enhanced in response to SMAP treatment (Fig 7E-G; S5D and E Fig). Collectively, these results support the potential therapeutic application of PP2A phosphatase reactivation and Akt kinase inhibition for the treatment of HCC with Aldob deficiency.

Discussion

Emerging studies have documented hepatic Aldob deficiency in HCC but the underlying mechanisms remain poorly defined. Our recent study uncovered a mechanism by which loss of Aldob led to a novel model of metabolic reprogramming through upregulation of glycolysis, PPP and TCA to promote HCC. This tumor promoting effect due to the loss of Aldob is achieved by releasing the inhibition on G6PD and PPP metabolism as a result of destabilizing Aldob/G6PD/p53 protein complex. However, the upstream signaling events are still unknown. In this study, we observe another non-enzymatic tumor-suppressive role of Aldob through a direct interaction with Akt in HCC, independent of Aldob enzymatic activity (Fig 8). Aldob inhibits Akt activity and downstream signaling events that leads to the impairment of cell cycle progression and metabolic flux to glycolysis and TCA cycle, thereby suppressing HCC cell proliferation and tumorigenesis. Furthermore, Aldob interacts with p-Akt to facilitate the recruitment of protein phosphatase PP2A and expedite PP2A-mediated dephosphorylation, resulting in attenuated Akt activity. On the other

hand, loss of Aldob or disruption of the Aldob/Akt interaction in Aldob mutation restores Akt activation, leading to cell cycle progression and upregulation of glucose metabolism though HK1 expression. Consistently, a reverse correlation of Aldob and p-Akt level is observed in human HCC tumor tissues and a combination of low Aldob expression with high p-Akt expression predicts the worst prognosis in HCC. Importantly, chemical inhibition of Akt kinase with MK2206 or reactivation of PP2A phosphatase activity with specific SMAP represses the tumorigenic effects resulting from the loss of Aldob *in vitro* and *in vivo*, further supporting the potential application of Akt inhibitors or PP2A activators for HCC treatment.

Dysregulated PI3K/Akt pathway contributes to multiple malignancies and it is of great clinical significance to characterize the molecular mechanisms leading to the hyperactivation of Akt signaling in carcinogenesis. In addition to the hepatitis virus infection and genomic alterations in PI3K/Akt pathway, emerging studies have focused on the novel protein interactions with Akt pathway members involved in the regulation of Akt kinase activity [44]. Here, we found that Aldob directly interacted with Akt resulting in reduced Akt phosphorylation. Although the kinase activity of Akt is critical for its interaction with Aldob, the enzymatic activity of Aldob plays a less important role in this regard. Interestingly, among these seven single mutants of Aldob, the mutant R304A significantly destroyed this interaction with Akt, leading to the restoration of Akt phosphorylation and cell growth. The active site residue R304 plays a crucial role in aldolase enzymatic mechanism and inactivating mutant at R304 residue causes HFI [45]. Although there is currently no human data linking HFI to HCC, our results warrant

future study on incidence of HCC in HFI populations, especially those with this mutation. On the other hand, three Akt isoforms (Akt1-3) exhibit over 80% identity at amino acid sequence, but are not functionally redundant based on different phenotypes observed by genetic deletion of each isoform in mice [3]. Akt1 played a crucial role in cell survival [46], while Akt2 maintained glucose homeostasis [47]. We found *ALDOB* KO significantly increased Akt2 phosphorylation at S474 site, and Aldob interacts with Akt2 in HCC cells, suggesting Aldob plays a similar role on regulating both Akt1 and Akt2 activity. Ongoing studies will examine the role of Aldob and its modulation of Akt isoform-specific signaling networks and biological outcomes.

Emerging studies have unveiled a pleotropic role of Aldolase in diverse physiological and pathological processes, in addition to the well-established role of glycolytic enzyme [12]. Our current work clearly demonstrates the great significance of Aldob-induced repression of Akt activity for the tumor-suppressive function of Aldob in HCC. Moreover, the inverse expression patterns of Aldob and p-Akt suggest that Aldob may be applied as a potential biomarker for HCC treatment with targeted Akt therapeutics. Our previous study identified a novel mechanism by which Aldob interacts with G6PD to reprogram metabolism in HCC. Here, we also highlight the role of Aldob in regulating glucose metabolism through inhibiting Akt activity. Extensive evidence indicates that activated Akt promotes glucose uptake and glycolysis through activating transcription factors and upregulating many glycolytic enzymes [18]. Akt increases the expression and activity of HK1 by activating HIF1α through stimulation of mTORC1 [48, 49]. Indeed, our studies showed that loss of Aldob upregulates entire central carbon

metabolism, including glycolysis, TCA and PPP, which was accompanied by activated Akt and increased HK1 expression. Moreover, Aldob-induced inhibition of Akt activity not only reduced glucose metabolic flux to glycolysis and TCA cycle, but also induced cell cycle arrest through downregulating Akt/GSK3β/CyclinD1 signaling, thereby leading to the impairment of cell proliferation. Thus these findings fully demonstrate the important tumor-suppressive role of Aldob through modulating Akt activity and its downstream signaling events.

Our current study has identified a close functional relationship among Aldob, Akt and PP2A, providing new mechanistic insights into the crucial upstream regulators involved in the Akt phosphorylation homeostasis mediated by the coordinate regulation by protein kinases and phosphatases [50]. As a tumor suppressor, PP2A negatively regulates several oncogenic signaling pathways and controls various cellular functions, such as cell growth, cell cycle and apoptosis [51]. PP2A-B55α has been shown to dephosphorylate Akt through a direct association and negatively regulate Akt-induced cell proliferation and survival [8]. Herein we demonstrated that Aldob was involved in PP2A-induced inhibition of Akt phosphorylation at both T308 and S473 sites. Indeed, we showed that downregulated Aldob attenuated PP2A interaction and dephosphorylation of Akt, which was consistent with the inverse relationship between Aldob and p-Akt expression in tumor tissues of human HCC and *ALDOB* KO mice. Furthermore, inhibition of PP2A restored Akt phosphorylation in Aldob-expressing cells, while PP2A reactivation using SMAP enhanced Aldob-induced inhibition of Akt phosphorylation. Moreover, alteration of Aldob expression had no effect on PP2AC

expression, and endogenous PP2AC was identified in Aldob immunocomplex. It is conceivable that Aldob interacts with p-Akt and functions as a scaffold protein to further recruit the serine/threonine phosphatase PP2A to its direct substrate Akt resulting in the inhibition of downstream Akt signaling.

Targeting key components of PI3K/Akt pathway is being explored as a therapeutic approach for cancer treatment. Several Akt small molecular inhibitors have entered different stages of clinical trials [3]. MK2206 is a potent and orally bioavailable allosteric inhibitor of Akt that specifically targets Akt inactive conformation and blocks PDK1-mediated phosphorylation and activation [21]. To date, MK2206 has shown moderate anti-tumor efficacy *in vitro* and in early clinical studies as a monotherapy, and exerts significantly more promising tumor inhibitory activities in combination with other agents, such as HCC first-line treatment sorafenib [52, 53]. Our data demonstrated that MK2206 treatment potently inhibited Akt phosphorylation and tumorigenic effects resulted from low Aldob level. Furthermore, tumor cells with low Aldob level were more responsive to Akt inhibition than those with high Aldob expression in which Akt signaling at baseline was already reduced. Collectively, our work indicates that targeting hyperactive Akt due to the loss of Aldob in HCC may be a viable therapeutic strategy.

In addition to direct inhibition of oncogenic kinases, stimulation of endogenous phosphatases to indirectly inactivate kinase signaling has been considered as a promising anticancer therapeutic approach. PP2A is functionally inactivated in many cancers, as a result of various mechanisms including somatic mutation, increased

expression of endogenous PP2A inhibitors and post-translational modifications of the catalytic subunit [39]. Aberrant transcripts of tumor suppressor gene *PPP2R1B* were detected in 29% of HCC tumors, which associated with the development of HCC [54]. Overall, the activation of PP2A has the potential to exert anti-tumor effect toward multiple oncogenic signaling proteins that drive cancer progression. FTY720 (fingolimod) has been reported to indirectly activate PP2A through inhibiting the endogenous PP2A inhibitor SET and exhibits high anti-tumor efficacy against HCC [38, 55]. In this study, we report that an orally bioavailable PP2A activator SMAP had anti-HCC activity *in vitro* and *in vivo* through its ability to simultaneously inhibit PP2A substrates Akt and ERK activity resulting in cell cycle arrest and ultimately cell death. SMAP mediated PP2A activation potentiated Aldob-induced suppression of Akt signaling and tumor growth. Our findings provide evidence that the restoration of PP2A tumor suppressive phosphatase activity could represent a novel targeted therapeutic approach for HCC treatment. Further studies exploring the therapeutic effects of PP2A reactivation in Aldob-defective cancers are therefore of critical importance.

In summary, our study uncovers the biological importance of Aldob-mediated Akt inhibition through the formation of Aldob/Akt/PP2A protein complex, independent of Aldob enzymatic activity. Our study suggests that targeting hyperactive Akt resulting from Aldob deficiency through directly inhibiting Akt kinase or reactivating PP2A phosphatase activity may serve as an anti-tumor treatment for HCC.

Methods

Mouse Models

For subcutaneous xenograft growth model, Huh7-Aldob or Vector cells (2×10^6) mixed in serum-free medium containing 50% Matrigel (BD Biosciences) were subcutaneously injected into the left and right flanks of 5-week-old male BALB/C nude mice. After 10 days, the mice were randomly assigned to control solvent and agent treatment groups (n=6 per group). MK2206 (40 mg/kg, once every other day) and SMAP (5 mg/kg, twice a day) were administered via oral gavage. Tumor growth and body weight were monitored every other day for 3 weeks. Tumor volume was estimated using the following formula: volume=0.52 × length × width^2. Animals were observed for signs of toxicity (weight loss, abdominal stiffness, and ruffled fur). Tumors were harvested, photographed and weighted 2 hours after the final dose of treatment, following snap-frozen in liquid nitrogen for immunoblotting or fixation in 4% paraformaldehyde (PFA) for immunohistochemistry. IHC staining was performed to examine the protein expression of proliferation marker gene Ki67 in the tumor tissues. Mice were housed in pathogen-free animal care facilities in Shanghai Institutes for Biological Sciences (SIBS), Chinese Academy Science (CAS) and allowed access to water and chow diet *ad libitum*. All animal experimental procedures were conformed to SIBS Guide for the Care and Use of Laboratory Animals and were approved by the Institutional Animal Care and Use Committee of SIBS, CAS.

Cell culture and HCC tissue samples

The human HCC cell lines Huh7 and HCC-LM3 were purchased from Cell Bank of CAS. Primary hepatocytes were isolated from the livers of male liver-specific *ALDOB*-knockout and WT mice using collagenase perfusion as previously described [56]. HCC cell lines and primary hepatocytes were cultured in Dulbecco's modified Eagle's medium (DMEM, Hyclone) plus with 10% fetal bovine serum (FBS, Hyclone) and 1% penicillin-streptomycin (Gibco) in a 37°C incubator with 5% CO2 in air. PVTT cell line CSQT2 was gifts from Dr. Cheng Shuqun.

Human HCC tissues were collected immediately after hepatectomy from the Eastern Hepatobiliary Surgery Hospital, Shanghai. Collection of patient specimens with informed consent to an established protocol and all experimental procedures were approved by the Research Ethics Committee of Eastern Hepatobiliary Surgery Hospital. The fresh specimens were snap-frozen in liquid nitrogen and stored at -80°C until analysis.

Reagents

MK2206 (Selleck Chemicals) was dissolved in DMSO (Sigma-Aldrich) and diluted in DMEM with a final concentration of 0.1 % DMSO for *in vitro* studies or in the vehicle solution containing Cremophor (Sigma-Aldrich), 95% ethanol and water in a ratio of 1:1:6 for *in vivo* studies. EGF (Sigma), insulin (Invitrogen) and okadaic acid (Cell Signaling Technology) were used at the indicated doses. The PP2A activator SMAP compound (provided by Goutham Narla, The University of Michigan, Ann Arbor, MI) was dissolved in DMSO and stored at room temperature and used for up to

1 month for *in vitro* studies. For *in vivo* studies, SMAP was prepared in a N, N-Dimethylacetamide (DMA)/Kolliphor HS-15 (Solutol)/diH_2O solution.

Plasmids and viruses

Aldob, Akt1 and Akt2 expression plasmids were constructed by cloning the open reading frame of each cDNA into the multiple cloning site of pCDNA3.0 vector, and their different Flag or Myc tag was constructed through design in one primer. The different gene fragments were amplified using their primers. The pcDNA3.0 vector and each PCR fragments were both digested with their restriction enzymes EcoRI and XhoI or BamHI and XhoI or EcoRI and XhoI, and then ligated with T4 ligase. Transformation was performed using DH5α competent cells. Single clones were selected and amplified to extract plasmids. All clones were sequenced to confirm the results. Flag-PP2A plasmids were obtained from Dr. Xie Dong (SIBS, CAS). Plasmid transfection and virus infection: Expression constructs were transfected into cells using Lipofectamine 2000 Transfection Reagent (Invitrogen) following the manufacturer's protocol. Lentivirus expression clone pLVX-IRES-GFP-puromycin-Aldob with/without Flag-tag was constructed with the Aldob fragment digested from pcDNA3.0-Aldob mentioned above via restriction enzyme EcoRI and XhoI. This fragment was inserted into pLVX-IRES-GFP-Puro vector and sequenced to verify the results. Lentivirus was produced by co-transfection of 293T cells using Lipofectamine 2000 Transfection Reagent (Invitrogen) with 3 μg pCMV-dR8.91, 2 μg pCMV-VSV-G and the target gene expression vectors (such as 5 μg pLVX-Aldob-Flag-puro). Fresh medium was

transferred into the dish after transfection of 6 hours. After 48h, the virus was harvested from the medium filtered by 0.45 mm Steriflipfilter (Millipore). Virus infection was carried out by incubating cells with cell medium containing indicated virus and 5 μg/ml polybrene (Sigma) for 8-12 hours. Cells were allowed to recover in complete medium for 24h and then selected with antibiotic (such as puromycin) for 10-15 days until stable cell lines were screened and constructed.

RNA-mediated interference (RNAi)

siRNA-Aldob-2-F: 5'-ACCCUCUACCAGAAGGACAdTdT-3', siRNA-Aldob-2-R: 5'-UGUCCUUCUGGUAGAGGGUdTdT-3', siRNA-Aldob-3-F: 5'-GUAUGUUCACACGGGUUCUdTdT-3', siRNA-Aldob-3-R: 5'-AGAACCCGUGUGAACAUACdTdT-3'. siRNA-Akt1-F: 5'-GCUACUUCCUCCUCAAGAAdTdT-3', siRNA-Akt1-R: 5'-UUCUUGAGGAGGAAGUAGCdTdT-3'. The siRNA was transfected into cells using Lipofectamine 2000 Transfection Reagent (Invitrogen) for at least 48 hours and then subjected to different assays.

Western blotting and antibodies

Cells or tissues were lysed in ice-cold lysis buffer (25 mM Tris pH 8.0, 150 mM NaCl, 1 mM $CaCl_2$, 1% Triton X-100) with EDTA-free protease inhibitors (Bimake) and phosphatase inhibitors (Bimake) and determined the protein concentration though BCA protein assay kit (Beyotime Biotechnology). Equal amounts of total protein were

subjected to 10% sodium dodecyl sulfate (SDS)-polyacrylamide gel electrophoresis (PAGE) and then transferred to polyvinylidene fluoride (PVDF, Millipore) membranes and incubated with the indicated antibodies. Antibodies to Aldob (18065-1-AP), GAPDH (60004-1-Ig), Tubulin (11224-1-AP), p70S6K (14485-1-AP), PHLPP (22789-1-AP), p21 (10355-1-AP), p27 (25614-1-AP), PDK1 (17086-1-AP), PP2AC (13482-1-AP), GST-tag (66001-2-AP), Hexokinase1 (19662-1-AP) were purchased from Proteintech. Antibodies to pT308-Akt (13038), pS473-Akt (4060), Akt1 (2938), pS9-GSK3β (5558), GSK3β (12456), pT389-S6K (9205), Myc-tag (2276), IgG (2729), pT202/Y204-ERK (4370), ERK (4695) were purchased from Cell Signaling Technology. Antibodies to Flag-tag (F3165) were purchased from Sigma. Antibodies to pT308-Akt (ab38449, for IHC use), CyclinD1 (ab16663), Ki67 (ab15580, for IHC use) were purchased from Abcam. After extensive rinse with TBST, immunoreactive bands were incubated with horseradish peroxidase (HRP)-conjugated secondary antibodies and visualized using a chemiluminescence (ECL) kit (Proteintech).

Cell viability assay

The viability assay was performed by seeding cells in a 96-well plate at a density of 2,000 cells/well for 6 repeats. After 7 hours, cell media were replaced with fresh media with various concentrations of test agents or control DMSO and cells were proceeded to grow. CCK8 (OBIO Cell Counting Kit) then was added to separate plates at the indicated time according to the manufacturer's instruction.

Colony formation assay

Colony formation assays were adapted from a protocol reported previously [33]. Cells of different groups were seeded (5000 cells/well) into six-well plates and cultured for 7-10 days. Medium were changed every other day. Colonies were washed with PBS, fixed with 10% acetic acid/10% methanol for 20 minutes, and then stained with 0.4% crystal violet in 20% ethanol for 20 minutes. After staining, the plates were washed and air-dried for colony visualization.

Cell cycle analysis

Cells of different groups were plated (2×10^5 cells/well) into six-well plates and subjected to indicated treatment. Resulting cells were detached with trypsin, washed with ice cold PBS, and fixed in 70% ethanol overnight. About 1×10^6 cells were detected using the cell cycle analysis kit (Beyotime Biotechnology, C1052). Then cells were incubated with propidium iodide (PI) and RNAase for 30 min at 37°C, followed by analysis via the flow cytometry (BD Bioscience). The results were presented as the proportion of cell population in each phase of the cell cycle which was determined using FlowJo 7.6 software (Treestar Inc., USA).

Metabolic flux experiments using [U-$^{13}C_6$]-glucose and Gas chromatography/mass spectrometry

Cells of different groups were seeded at a density of approximately 2×10^6 cells per 10 cm dish. After cells grew to ~60 % confluence, the unlabeled medium was replaced

with [U-$^{13}C_6$]-glucose medium which composed of low glucose DMEM (Gibco, 11054-020: 1g/L unlabeled glucose, no glutamine) with supplement of 1g/L [U-$^{13}C_6$]-glucose (Cambridge Isotope Laboratory), 10% (v/v) fetal bovine serum, the 1mM pyruvate, the unlabeled 2mM L-glutamine, and 1% (v/v) penicillin-streptomycin with or without MK2206 treatment (5 μM). At this point, it was regarded as t = 0 h. The labeling time of [U-$^{13}C_6$]-glucose for 12 hours. [U-$^{13}C_6$]-glucose medium samples after cell culture were collected at 0 h and 12 h, and stored at -80°C immediately for later analysis. Then we quickly removed the medium completely and immediately put plates on dry ice and added 700 μl of 50% (vol/vol) methanol (precooled at -80°C) for 20 minutes. Next the cell lysate/methanol mixtures were totally scraped from the plates and transferred to 2 ml tubes. We added 500μl chloroform into the tubes, then vortexed the tubes and centrifuged at 14,000 g for 15 minutes at 4 °C. The supernatants were transferred into new tubes and lyophilized in a vacuum concentrator. Then add 70μl O-Isobutylhydroxylamine Hydrochloride (TCI, 20 mg/ml) to the dried pellet and incubate at 85°C in metal bath for 20 minutes. After cooling, add 30 μl N-tert-Butyldimethylsilyl-N-Methyltrifluoroacetamide (Sigma) to incubate at 85°C for 1 hours before centrifugation at 14,000 g for 15 minutes at 4°C. The supernatant was transferred to an autosampler vial for GC/MS analysis.

A Shimadzu QP-2010 Ultra GC-MS was programmed as described previously [57] with an injection temperature of 250°C. 1 μl of sample was injected with an injection split ratio of 1/10. GC oven temperature started at 110°C for 4 min, rising to 230°C at 3°C/min and to 280°C at 20°C /min with a final holding at this temperature for 2 min.

GC flow rate with helium carrier gas was 50 cm/s. The GC column used was a 30 m x 0.25 mm x 0.25 mm HP-5ms. GC-MS interface temperature was 300°C and (electron impact) ion source temperature was set at 200°C, with 70 V/150 μA ionization voltage/current. The mass spectrometer was set to scan m/z range 50-800, with 1 kV detector. GC/MS data were analyzed to determine isotope labeling and quantities of metabolites and implemented in MATLAB [58]. To determine ^{13}C labeling, the mass distribution for known fragments of metabolites was extracted from the appropriate chromatographic peak. Labeling results are expressed as average fraction the particular compound that contains isotopic label from the particular precursor.

Immunoprecipitation (IP) and GST pull-down assay

1000 μg cell lysates were incubated with the indicated antibody (1-2μg) overnight at 4°C with gentle rotation, followed by 6 hours incubation with Protein A/G Sepharose beads (Santa Cruz). Then beads were washed 4 times with IP lysis buffer (150mM Tris-HCl, 400mM NaCl, 0.8%Triton X-100, pH 7.4) and boiled in sample buffer before being resolved by SDS-PAGE and immunoblotted with indicated antibodies. For the Flag or Myc-tag labeled IP experiments, cell lysates were incubated with antibody-Flag or antibody-Myc affinity gel (Bimake) overnight at 4°C. Affinity gel were collected after 300g centrifuging for 4 min at 4°C, and then washed 4 times. The subsequent operations were similar to western blot analysis. For GST pull-down assay, recombinant GST-Akt1 or GST proteins was incubated with His-Aldob proteins or cell lysates derived from cells transfected with indicated constructs in binding buffer (25 mM Tris-

HCl, 200 mM NaCl, 1 mM EDTA, 0.5% NP-40, 10 μg/μl BSA, 1 mM DTT, pH 7.3). 100μl prepared Glutathione Sepharose 4B (GE Healthcare) were added to the mixture and incubated overnight. After washed in ice-cold binding buffer for three times, bound proteins were released by boiling in sample buffer and resolved by SDS-PAGE electrophoresis.

Expression and purification of recombinant proteins

The full-length Aldob and Akt1 genes were inserted into the pET-30a (Novagen) and pGEX4T1 (GE Healthcare) expression plasmids, respectively. The E. coli BL21 (DE3) Codon-Plus strain (Novagen) transformed with the reconstructed expression plasmid was cultured at 37 °C in LB medium containing 0.05 mg/ml ampicillin until OD600 of medium reached 0.8, and addition of 0.1 mM IPTG induced the target protein expression at 16 °C for 24 hours. The cells were further harvested by centrifugation and lysed by sonication in the lysis buffer (20 mM Tris-HCl, 300 mM NaCl, and 1 mM PMSF). The recombinant proteins were purified using GSH Magnetic Beads for GST tag protein purification (Bimake, B23702) and Nickel Magnetic Beads for His tag protein purification (Bimake, B23602) according to the manufacturer's protocol. The purified proteins were determined by SDS-PAGE with high purity (> 95%).

In vitro Akt kinase assay

The *in vitro* kinase assay (Abcam, ab65786) was performed according to the manufacturer's instructions. Cell lysates were immunoprecipitated with either anti-

Akt1 or anti-IgG antibody along with protein A/G beads overnight and the immunoprecipitates were incubated with substrate GSK3α Protein/ATP mixture in kinase reaction buffer for 30 min at 30 °C. The reactions were terminated by 6×SDS loading buffer and subjected to western blot analysis with antibody against pS21-GSK3α.

In vitro PP2A dephosphorylation assay

The *in vitro* PP2A dephosphorylation assay was performed using phosphorylated Myc-Akt1 as the substrate. Myc-Akt1 transfected Huh7 cells were serum-starved for 24 hours and then stimulated with 0.1μM insulin for 1 hour before harvesting. Equal amounts of cell lysates were incubated with antibody-Myc affinity gel overnight at 4°C. The immunoprecipitates were washed 3 times in IP lysis buffer, 3 times in PP2A phosphatase assay buffer (20 mM HEPES pH 7.2, 100 mM NaCl and 3 mM DTT) and finally resuspended in PP2A phosphatase assay buffer. Then immunoprecipitated phospho-Akt were reacted with recombinant active PP2A (BPS Bioscience, 30056) at 30 °C for indicated time periods in the presence or absence of recombinant WT-Aldob or Aldob-R304A mutant. Dephosphorylation reactions were terminated by 6×SDS loading buffer and subjected to western blot analysis.

Tissue microarray and Immunohistochemistry

Immunohistochemistry was constructed on the tissue microarray (TMA) with a two-step immunoperoxidase technique [59]. In short, tissues were fixed overnight in 4%

paraformaldehyde (PFA), then dehydrated in ethanol and embedded in paraffin. The paraffin-embedded tissue pieces were cut into 5-micron thick sections, which were stained with hematoxylin and eosin (H&E) and processed for IHC. For IHC, specimen sections were dewaxed, rehydrated in ethanol, and subjected to antigen extraction. Endogenous peroxidase activity was blocked with 0.3% hydrogen peroxide in methanol for 30 min. Sections were blocked by 2% BSA in PBS for 1 hour at 37 °C, and then incubated with the indicated primary antibody overnight at 4°C. After washing 3 times with PBS the next day, the samples were further incubated for 1 hour at 37 °C using the corresponding secondary antibodies. The slides were displayed by DAB staining. IHC slides and tissue microarrays were read using Vectra 2 (Perkin Elmer) to quantify protein expression in all samples. For tissue microarrays, protein expression intensity was stratified into negative, weak, moderate and strong. The scoring formula was (weak + moderate + strong)/ (negative + weak + moderate + strong) × 100%. Representative images of different expression intensities of Aldob and p-Akt in HCC were shown in Fig 1B. For tissue IHC, IHC staining of tumor tissue was performed (IHC score = intensity × area). The intensity was graded as 0, negative; 1, weak; 2, moderate; and 3, strong. The staining areas of 0, 1-25%, 26-50%, 51-75% and 76-100% were 0, 1, 2, 3 and 4, respectively.

Statistical analysis

All data are presented as the means ± standard errors of the mean from at least 3 independent experiments. The survival curve was calculated according to the Kaplan-

Meier method and differences were assessed by the Log-rank test. Differences between measurable variants of two groups were calculated by the unpaired Student's t-test or 2-way ANOVA using GraphPad Prism 5.0, and the value of $p<0.05$ was considered statistically significant.

Abbreviations

HCC, Hepatocellular carcinoma; Aldob, Fructose-1, 6-bisphosphate aldolase B; p-Akt, Phosphorylated Akt; PP2A, Protein phosphatase 2A; SMAP, Small molecule activator of PP2A; ERK, Extracellular signal-regulated kinase; PDK1, Phosphoinositide-dependent kinase 1; GSK-3, Glycogen synthase kinase-3; HK1，Hexokinase 1; EGF, Epidermal growth factor; TCA cycle, Tricarboxylic acid cycle; HFI, Hereditary fructose intolerance.

Declarations

Ethics approval and consent to participate

This study was approved by the Clinical Research Ethics Committee of the Eastern Hepatobiliary Surgery Hospital, Shanghai, China. Written informed consent was obtained from all patients. All specimens were pathologically confirmed at the Eastern Hepatobiliary Surgery Hospital. Animal studies were approved by the Institutional Animal Care and Use Committee of the Shanghai Institutes for Biological Sciences of the Chinese Academy of Sciences (approval number 2015-AN-2).

Data Availability Statement

All relevant data are within the paper and its Supporting Information files.

Funding

This work was financially supported by National Key R&D Program of China

administered by Chinese Ministry of Science and Technology (MOST) (2016YFD0400205), the National Natural Science Foundation of China (31671231 and 91857112).

Competing interests

The Icahn School of Medicine at Mount Sinai has filed patents covering composition of matter on the small molecules disclosed herein for the treatment of human cancer and other diseases (International Application Numbers: PCT/US15/19770, PCT/US15/19764; and US Patent: US 9,540,358 B2). Mount Sinai is actively seeking commercial partners for the further development of the technology. G.N. has a financial interest in the commercialization of the technology.

Acknowledgements

We thank Dr. Dong Xie (Shanghai Institute of Nutrition and Health, Chinese Academy of Sciences, Shanghai, China) for critical technical support. We acknowledge the help from molecular biology core laboratory, animal facilities, and mass spectrometry facilities at Shanghai Institutes of Nutrition and Health (SINH), CAS, Shanghai.

Author Contributions

Conceptualization: Xuxiao He, Huiyong Yin.

Methodology: Xuxiao He, Min Li, Huiyong Yin.

Investigation: Xuxiao He, Min Li, Guijun Liu, Ningning Wang, Chunzhao Yin, Qiaochu Tu, Hongming Yu.

Writing: Xuxiao He, Goutham Narla, Huiyong Yin.

Funding acquisition: Goutham Narla, Yongzhen Tao, Shuqun Cheng, Huiyong Yin.

Resources: Goutham Narla, Hongming Yu, Shuqun Cheng.

Supervision: Yongzhen Tao, Huiyong Yin.

Contact Information for the Corresponding Author

Huiyong Yin, Ph.D; Shanghai Institute of Nutrition and Health, Chinese Academy of Sciences; 320 Yueyang Road, Shanghai, China 200031; Phone: (86)-21-54920942; E-mail: hyyin@sibs.ac.cn

References

1. Villanueva A. Hepatocellular Carcinoma. N Engl J Med. 2019;380(15):1450-1462.

2. Burkhart RA, Ronnekleiv-Kelly SM, Pawlik TM. Personalized therapy in hepatocellular carcinoma: Molecular markers of prognosis and therapeutic response. Surgical oncology. 2017;26(2):138-145.

3. Manning BD, Toker A. AKT/PKB Signaling: Navigating the Network. Cell. 2017;169(3):381-405.

4. Fruman DA, Chiu H, Hopkins BD, Bagrodia S, Cantley LC, Abraham RT. The PI3K Pathway in Human Disease. Cell. 2017;170(4):605-635.

5. Szymonowicz K, Oeck S, Malewicz NM, Jendrossek V. New Insights into Protein Kinase B/Akt Signaling: Role of Localized Akt Activation and Compartment-Specific Target Proteins for the Cellular Radiation Response. Cancers (Basel). 2018;10(3).

6. Elstrom RL, Bauer DE, Buzzai M, Karnauskas R, Harris MH, Plas DR, et al. Akt stimulates aerobic glycolysis in cancer cells. Cancer Res. 2004;64(11):3892-3899.

7. Robey RB, Hay N. Is Akt the "Warburg kinase"?-Akt-energy metabolism interactions and oncogenesis. Seminars in cancer biology. 2009;19(1):25-31.

8. Kuo YC, Huang KY, Yang CH, Yang YS, Lee WY, Chiang CW. Regulation of phosphorylation of Thr-308 of Akt, cell proliferation, and survival by the B55alpha regulatory subunit targeting of the protein phosphatase 2A holoenzyme to Akt. The Journal of biological chemistry. 2008;283(4):1882-1892.

9. Gao TY, Furnari F, Newton AC. PHLPP: A phosphatase that directly dephosphorylates akt, promotes apoptosis, and suppresses tumor growth. Molecular

cell. 2005;18(1):13-24.

10. Salvatore F, Izzo P, Paolella G. Aldolase gene and protein families: structure, expression and pathophysiology. Horizons in biochemistry and biophysics. 1986;8:611-665.

11. Oppelt SA, Sennott EM, Tolan DR. Aldolase-B knockout in mice phenocopies hereditary fructose intolerance in humans. Molecular genetics and metabolism. 2015;114(3):445-450.

12. Chang YC, Yang YC, Tien CP, Yang CJ, Hsiao M. Roles of Aldolase Family Genes in Human Cancers and Diseases. Trends in endocrinology and metabolism: TEM. 2018;29(8):549-559.

13. Zhang CS, Hawley SA, Zong Y, Li MQ, Wang ZC, Gray A, et al. Fructose-1,6-bisphosphate and aldolase mediate glucose sensing by AMPK. Nature. 2017;548(7665):112-+.

14. Hu H, Juvekar A, Lyssiotis CA, Lien EC, Albeck JG, Oh D, et al. Phosphoinositide 3-Kinase Regulates Glycolysis through Mobilization of Aldolase from the Actin Cytoskeleton. Cell. 2016;164(3):433-446.

15. Kinoshita M, Miyata M. Underexpression of mRNA in human hepatocellular carcinoma focusing on eight loci. Hepatology. 2002;36(2):433-438.

16. Peng SY, Lai PL, Pan HW, Hsiao LP, Hsu HC. Aberrant expression of the glycolytic enzymes aldolase B and type II hexokinase in hepatocellular carcinoma are predictive markers for advanced stage, early recurrence and poor prognosis. Oncol Rep. 2008;19(4):1045-1053.

17. Tao QF, Yuan SX, Yang F, Yang S, Yang Y, Yuan JH, et al. Aldolase B inhibits metastasis through Ten-Eleven Translocation 1 and serves as a prognostic biomarker in hepatocellular carcinoma. Mol Cancer. 2015;14.

18. Cairns RA, Harris IS, Mak TW. Regulation of cancer cell metabolism. Nature reviews Cancer. 2011;11(2):85-95.

19. Zhu J, Thompson CB. Metabolic regulation of cell growth and proliferation. Nature reviews Molecular cell biology. 2019;20(7):436-450.

20. Jang M, Kim SS, Lee J. Cancer cell metabolism: implications for therapeutic targets. Experimental & molecular medicine. 2013;45:e45.

21. Hirai H, Sootome H, Nakatsuru Y, Miyama K, Taguchi S, Tsujioka K, et al. MK-2206, an allosteric Akt inhibitor, enhances antitumor efficacy by standard chemotherapeutic agents or molecular targeted drugs in vitro and in vivo. Molecular cancer therapeutics. 2010;9(7):1956-1967.

22. Hanahan D, Weinberg RA. Hallmarks of cancer: the next generation. Cell. 2011;144(5):646-674.

23. Warburg O. On the origin of cancer cells. Science. 1956;123(3191):309-314.

24. Anderson NM, Mucka P, Kern JG, Feng H. The emerging role and targetability of the TCA cycle in cancer metabolism. Protein & cell. 2018;9(2):216-237.

25. Weinberg SE, Chandel NS. Targeting mitochondria metabolism for cancer therapy. Nature chemical biology. 2015;11(1):9-15.

26. Coffee EM, Tolan DR. Mutations in the promoter region of the aldolase B gene that cause hereditary fructose intolerance. J Inherit Metab Dis. 2010;33(6):715-725.

27. Dalby AR, Tolan DR, Littlechild JA. The structure of human liver fructose-1,6-bisphosphate aldolase. Acta Crystallogr D. 2001;57:1526-1533.

28. Choi KH, Shi J, Hopkins CE, Tolan DR, Allen KN. Snapshots of catalysis: the structure of fructose-1,6-(bis)phosphate aldolase covalently bound to the substrate dihydroxyacetone phosphate. Biochemistry. 2001;40(46):13868-13875.

29. Esposito G, Santamaria R, Vitagliano L, Ieno L, Viola A, Fiori L, et al. Six novel alleles identified in Italian hereditary fructose intolerance patients enlarge the mutation spectrum of the aldolase B gene. Human mutation. 2004;24(6):534.

30. Esposito G, Imperato MR, Ieno L, Sorvillo R, Benigno V, Parenti G, et al. Hereditary fructose intolerance: functional study of two novel ALDOB natural variants and characterization of a partial gene deletion. Human mutation. 2010;31(12):1294-1303.

31. Resjo S, Goransson O, Harndahl L, Zolnierowicz S, Manganiello V, Degerman E. Protein phosphatase 2A is the main phosphatase involved in the regulation of protein kinase B in rat adipocytes. Cellular signalling. 2002;14(3):231-238.

32. Rocher G, Letourneux C, Lenormand P, Porteu F. Inhibition of B56-containing protein phosphatase 2As by the early response gene IEX-1 leads to control of Akt activity. The Journal of biological chemistry. 2007;282(8):5468-5477.

33. Guo J, Chakraborty AA, Liu P, Gan W, Zheng X, Inuzuka H, et al. pVHL suppresses kinase activity of Akt in a proline-hydroxylation-dependent manner. Science. 2016;353(6302):929-932.

34. Aoki M, Batista O, Bellacosa A, Tsichlis P, Vogt PK. The akt kinase: molecular

determinants of oncogenicity. Proceedings of the National Academy of Sciences of the United States of America. 1998;95(25):14950-14955.

35. Pim D, Massimi P, Dilworth SM, Banks L. Activation of the protein kinase B pathway by the HPV-16 E7 oncoprotein occurs through a mechanism involving interaction with PP2A. Oncogene. 2005;24(53):7830-7838.

36. Cohen P, Holmes CFB, Tsukitani Y. Okadaic Acid - a New Probe for the Study of Cellular-Regulation. Trends in biochemical sciences. 1990;15(3):98-102.

37. Perrotti D, Neviani P. Protein phosphatase 2A: a target for anticancer therapy. The Lancet Oncology. 2013;14(6):e229-238.

38. Sangodkar J, Farrington CC, McClinch K, Galsky MD, Kastrinsky DB, Narla G. All roads lead to PP2A: exploiting the therapeutic potential of this phosphatase. The FEBS journal. 2016;283(6):1004-1024.

39. O'Connor CM, Perl A, Leonard D, Sangodkar J, Narla G. Therapeutic targeting of PP2A. The international journal of biochemistry & cell biology. 2018;96:182-193.

40. Sangodkar J, Perl A, Tohme R, Kiselar J, Kastrinsky DB, Zaware N, et al. Activation of tumor suppressor protein PP2A inhibits KRAS-driven tumor growth. J Clin Invest. 2017;127(6):2081-2090.

41. Umesalma S, Kaemmer CA, Kohlmeyer JL, Letney B, Schab AM, Reilly JA, et al. RABL6A inhibits tumor-suppressive PP2A/AKT signaling to drive pancreatic neuroendocrine tumor growth. J Clin Invest. 2019;130:1641-1653.

42. McClinch K, Avelar RA, Callejas D, Izadmehr S, Wiredja D, Perl A, et al. Small-Molecule Activators of Protein Phosphatase 2A for the Treatment of Castration-

Resistant Prostate Cancer. Cancer Res. 2018;78(8):2065-2080.

43. Kauko O, O'Connor CM, Kulesskiy E, Sangodkar J, Aakula A, Izadmehr S, et al. PP2A inhibition is a druggable MEK inhibitor resistance mechanism in KRAS-mutant lung cancer cells. Sci Transl Med. 2018;10(450).

44. Franke TF. Intracellular Signaling by Akt: Bound to Be Specific. Sci Signal. 2008;1(24).

45. Choi KH, Mazurkie AS, Morris AJ, Utheza D, Tolan DR, Allen KN. Structure of a fructose-1,6-bis(phosphate) aldolase liganded to its natural substrate in a cleavage-defective mutant at 2.3 A(,). Biochemistry. 1999;38(39):12655-12664.

46. Cho H, Thorvaldsen JL, Chu QW, Feng F, Birnbaum MJ. Akt1/PKB alpha is required for normal growth but dispensable for maintenance of glucose homeostasis in mice. Journal of Biological Chemistry. 2001;276(42):38349-38352.

47. Cho H, Mu J, Kim JK, Thorvaldsen JL, Chu QW, Crenshaw EB, et al. Insulin resistance and a diabetes mellitus-like syndrome in mice lacking the protein kinase Akt2 (PKB beta). Science. 2001;292(5522):1728-1731.

48. Gordan JD, Thompson CB, Simon MC. HIF and c-Myc: sibling rivals for control of cancer cell metabolism and proliferation. Cancer Cell. 2007;12(2):108-113.

49. Sengupta S, Peterson TR, Sabatini DM. Regulation of the mTOR complex 1 pathway by nutrients, growth factors, and stress. Molecular cell. 2010;40(2):310-322.

50. Janssens V, Goris J. Protein phosphatase 2A: a highly regulated family of serine/threonine phosphatases implicated in cell growth and signalling. The Biochemical journal. 2001;353(Pt 3):417-439.

51. Seshacharyulu P, Pandey P, Datta K, Batra SK. Phosphatase: PP2A structural importance, regulation and its aberrant expression in cancer. Cancer Lett. 2013;335(1):9-18.

52. Yap TA, Yan L, Patnaik A, Fearen I, Olmos D, Papadopoulos K, et al. First-in-Man Clinical Trial of the Oral Pan-AKT Inhibitor MK-2206 in Patients With Advanced Solid Tumors. J Clin Oncol. 2011;29(35):4688-4695.

53. Chen KF, Feng WC, Hsu CH, Chen PJ, Cheng AL. Activation of PI3K/Akt signaling pathway mediates acquired resistance to sorafenib in hepatocellular carcinoma cells. Molecular cancer therapeutics. 2009;8(12).

54. Chou HC, Chen CH, Lee HS, Lee CZ, Huang GT, Yang PM, et al. Alterations of tumour suppressor gene PPP2R1B in hepatocellular carcinoma. Cancer Lett. 2007;253(1):138-143.

55. Omar HA, Chou CC, Berman-Booty LD, Ma Y, Hung JH, Wang D, et al. Antitumor effects of OSU-2S, a nonimmunosuppressive analogue of FTY720, in hepatocellular carcinoma. Hepatology. 2011;53(6):1943-1958.

56. Pei L, Waki H, Vaitheesvaran B, Wilpitz DC, Kurland IJ, Tontonoz P. NR4A orphan nuclear receptors are transcriptional regulators of hepatic glucose metabolism. Nature medicine. 2006;12(9):1048-1055.

57. Ma L, Tao Y, Duran A, Llado V, Galvez A, Barger JF, et al. Control of nutrient stress-induced metabolic reprogramming by PKCzeta in tumorigenesis. Cell. 2013;152(3):599-611.

58. Portnoy VA, Scott DA, Lewis NE, Tarasova Y, Osterman AL, Palsson BO. Deletion

of genes encoding cytochrome oxidases and quinol monooxygenase blocks the aerobic-anaerobic shift in Escherichia coli K-12 MG1655. Applied and environmental microbiology. 2010;76(19):6529-6540.

59. Cai X, Zhai J, Kaplan DE, Zhang YJ, Zhou LN, Chen XT, et al. Background progenitor activation is associated with recurrence after hepatectomy of combined hepatocellular-cholangiocarcinoma. Hepatology. 2012;56(5):1804-1816.

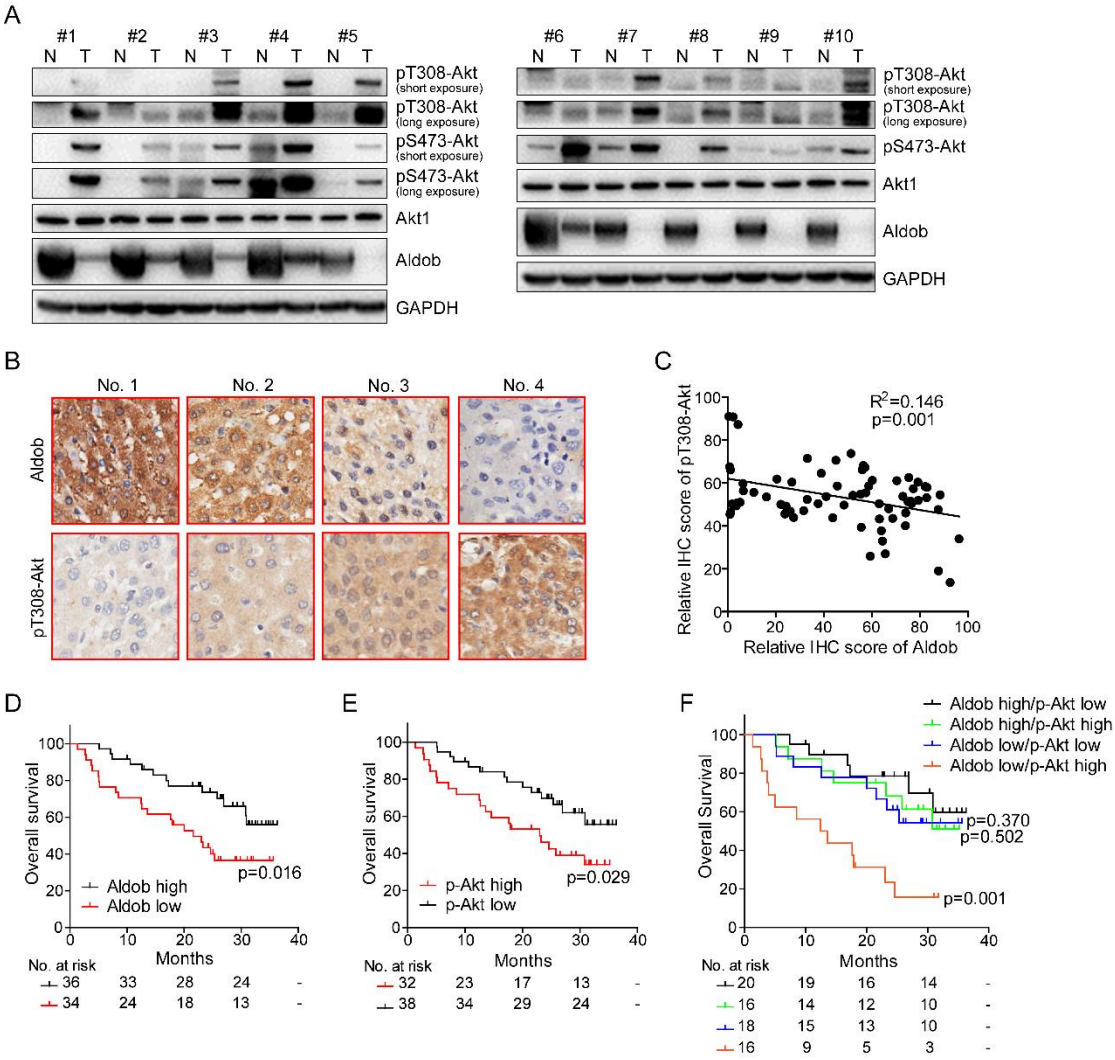

Fig 1. A negative correlation between Aldob and p-Akt expression in human HCC specimens.

(A) Immunoblot (IB) analysis of whole cell lysates (WCL) derived from 10 pairs of human HCC tumors and matched adjacent nonmalignant tissues. **(B)** Representative Immunohistochemistry (IHC) staining images of Aldob and pT308-Akt from the same HCC patients on tissue microarray were shown (original magnification ×200). **(C)** The relative IHC score of Aldob and pT308-Akt from tissue microarray of 70 HCC patients was plotted and assessed by a linear regression analysis. (**D** and **E)** Overall survival of 70 HCC patients grouped by high IHC score (≥50) or low IHC score (<50) of Aldob **(D)** or pT308-Akt **(E)** expression levels were conducted through the Kaplan-Meier analysis and Log-rank test. The number of patients at risk was listed below each curve. **(F)** Overall survival of 70 HCC patients grouped by different combination of Aldob and pT308-Akt levels were conducted through the Kaplan-Meier analysis and Log-rank test. The number of patients at risk was listed under each curve.

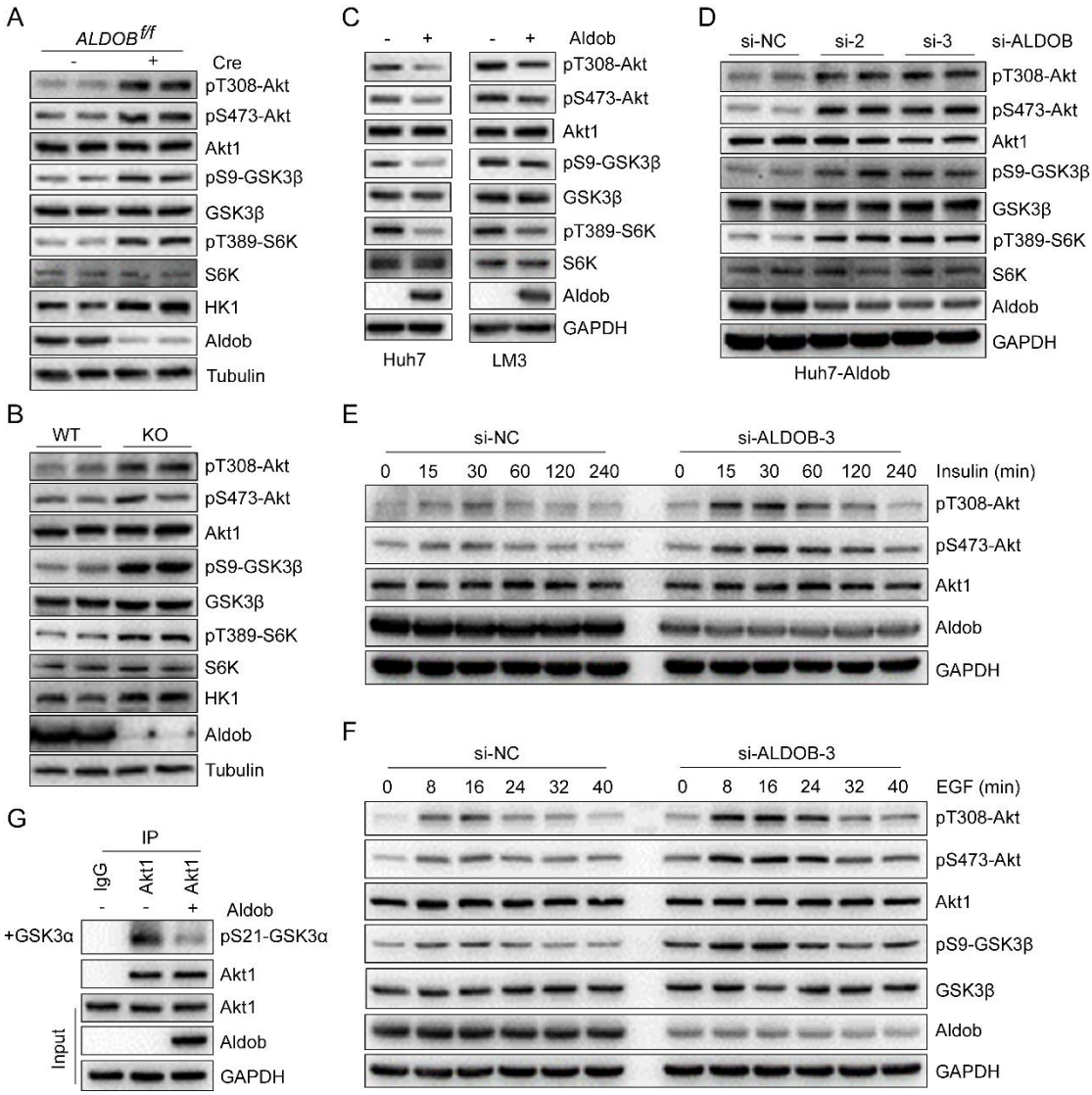

Fig 2. Aldob suppresses Akt phosphorylation and kinase activity.

(A) IB analysis of WCL derived from conditional *ALDOB* KO and WT mouse primary hepatocytes. **(B)** IB analysis of WCL derived from liver tissues of *ALDOB* KO and WT mice after injection with DEN at post-natal day 14 to induce hepatocellular carcinoma for 10 months. **(C)** IB analysis of WCL derived from Huh7 and LM3 cells stably expressing Aldob via lentiviral infection (with Vector as a negative control). **(D)** IB analysis of WCL derived from Aldob-overexpressing Huh7 (Huh7-Aldob) cells transfected with indicated siRNAs (si-NC as a negative control). **(E** and **F)** IB analysis of WCL derived from Huh7-Aldob cells transfected with indicated siRNAs. Resulting cells were serum-starved for 24 hours and then stimulated with 0.1 μM insulin **(E)** or 100 ng/ml EGF **(F)** at the indicated time before harvesting. **(G)** *In vitro* Akt1 kinase assay was conducted with recombinant GSK3α as a substrate and immunoprecipitated Akt1 from Huh7-Vector or Huh7-Aldob cells as the source of kinase. IgG was used as a negative control.

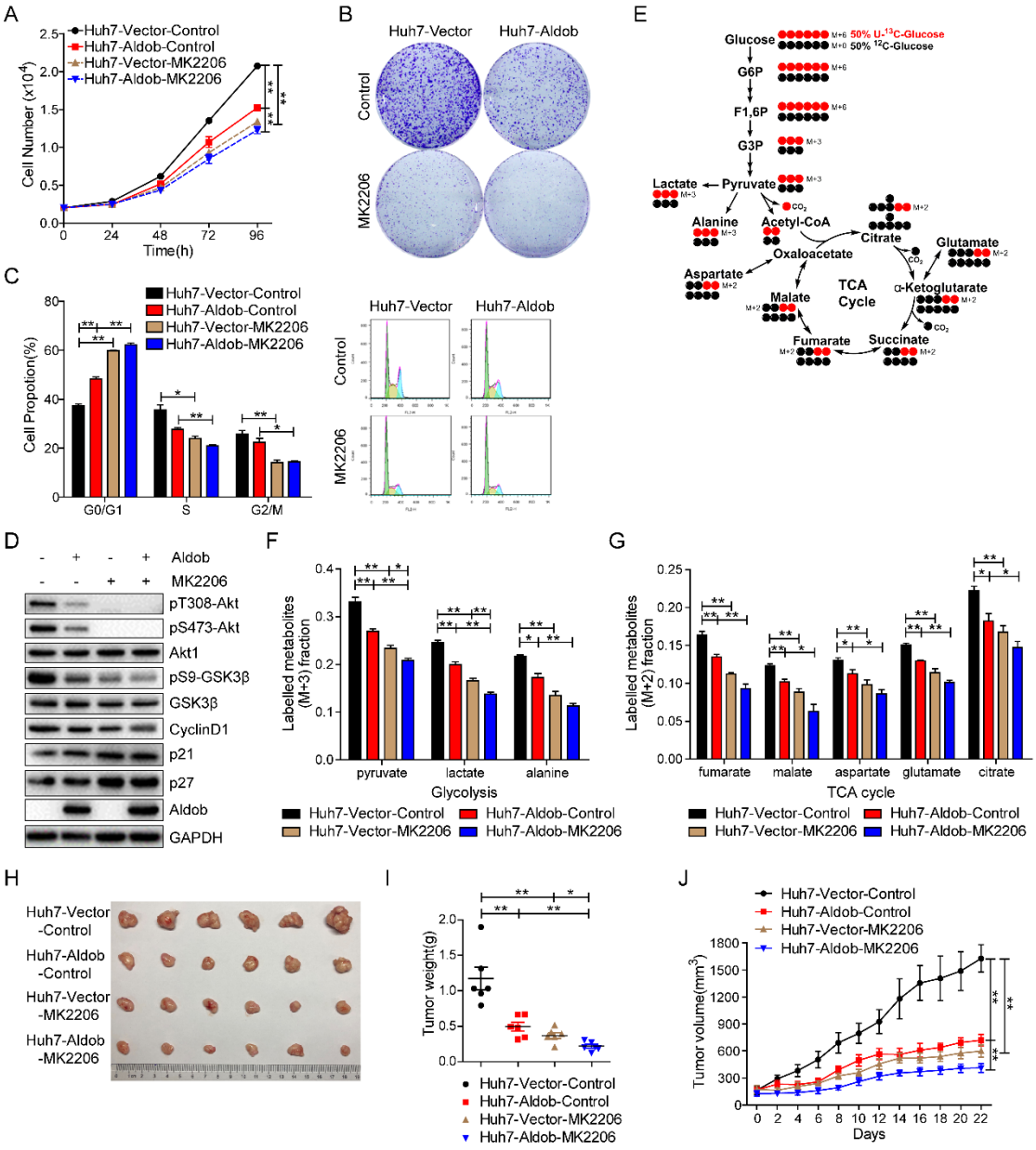

Fig 3. Aldob-mediated inhibition of Akt activity is required for Aldob-induced tumor-suppressive effects.

(A) Huh7-Vector and Huh7-Aldob cells were treated with DMSO or MK2206 (2 μM) at the indicated time and cell viability was measured by CCK-8 assays. **(B)** Huh7-Vector and Huh7-Aldob cells (5000 cells/well in 6-well plates) were cultured with or without MK2206 (2 μM) for 10 days before being fixed and stained. Representative graphs of cell colonies were shown. **(C** and **D)** Cells were treated with DMSO or MK2206 (2 μM) for 48 hours, and then monitored for cell cycle distribution by FACS **(C)** or subjected to IB analysis with the indicated antibodies **(D)**. **(E)** Schematic presentation of ^{13}C distribution in glycolysis and the first turn of the TCA cycle with

50% U-^{13}C-glucose (labeled at all six carbons, red circles) and 50% ^{12}C-glucose (unlabeled, black circles). G6P, glucose-6-phosphate; F1,6P, fructose-1,6-bisphosphate; G3P, glyceraldehyde-3-phosphate. (**F** and **G**) Fraction of the labeled metabolites of M+3 from ^{13}C-glucose in glycolysis **(F)** and fraction of the labeled metabolites of M+2 from ^{13}C-glucose in TCA cycle **(G)** by DMSO or MK2206 (5 μM) treatment for 12 hours in Huh7-Vector and Huh7-Aldob cells. **(H-J)** Huh7-Vector and Huh7-Aldob cells were injected subcutaneously into the flanks of nude mice, followed by treatment with Control solvent or MK2206 (n=6 mice). Representative tumor images **(H)**, xenograft tumor weight **(I)** and tumor size **(J)** in each group were recorded. Data are presented as mean ± SEM. * $p < 0.05$; ** $p < 0.01$ (Student's t-test).

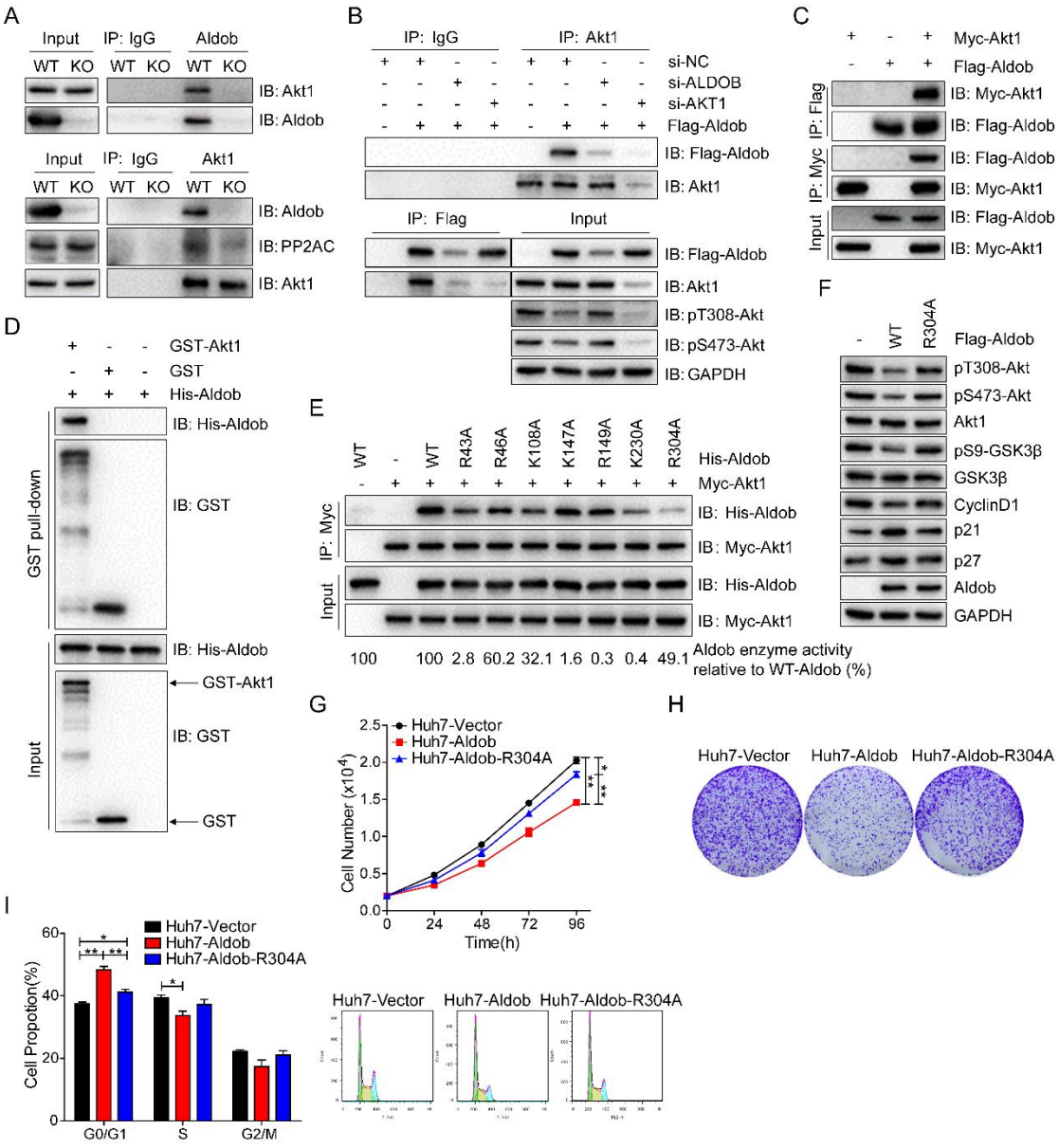

Fig 4. The direct interaction of Aldob with Akt is essential for Aldob to suppress Akt activity and HCC cell growth.

(A) IB analysis of endogenous anti-Aldob and anti-Akt1 co-immunoprecipitations (co-IP) and WCL derived from liver tissues of *ALDOB* KO and WT mice. IgG was used as a negative control. **(B)** IB analysis of anti-Akt1 and anti-Flag immunoprecipitation (IP) and WCL derived from Huh7 cells transfected with the indicated constructs and siRNAs. IgG was used as a negative control. **(C)** IB analysis of co-IP and WCL derived from Huh7 cells transfected with the indicated constructs. **(D)** GST pull-down analysis to demonstrate the direct interaction between recombinant proteins GST-Akt1 and His-Aldob. Recombinant GST protein was used as a negative control. **(E)** IP analysis was

performed with WCL derived from Myc-Akt1 transfected Huh7 cells and recombinant protein WT-His-Aldob or their various His-Aldob mutants harboring a lysine or arginine to alanine mutation in the identified active site residues of Aldob. The Aldob enzyme activity in Aldob mutants relative to WT-His-Aldob were calculated (bottom). **(F)** IB analysis of WCL derived from Huh7 cells transfected with WT or R304A mutant form of Flag-Aldob constructs. **(G-I)** Huh7 cells transfected with the indicated constructs were used to determine their effects on cell proliferation **(G)**, colony formation **(H)** and cell cycle distribution **(I)**. Data are presented as mean ± SEM. * $p < 0.05$; ** $p < 0.01$ (Student's t-test).

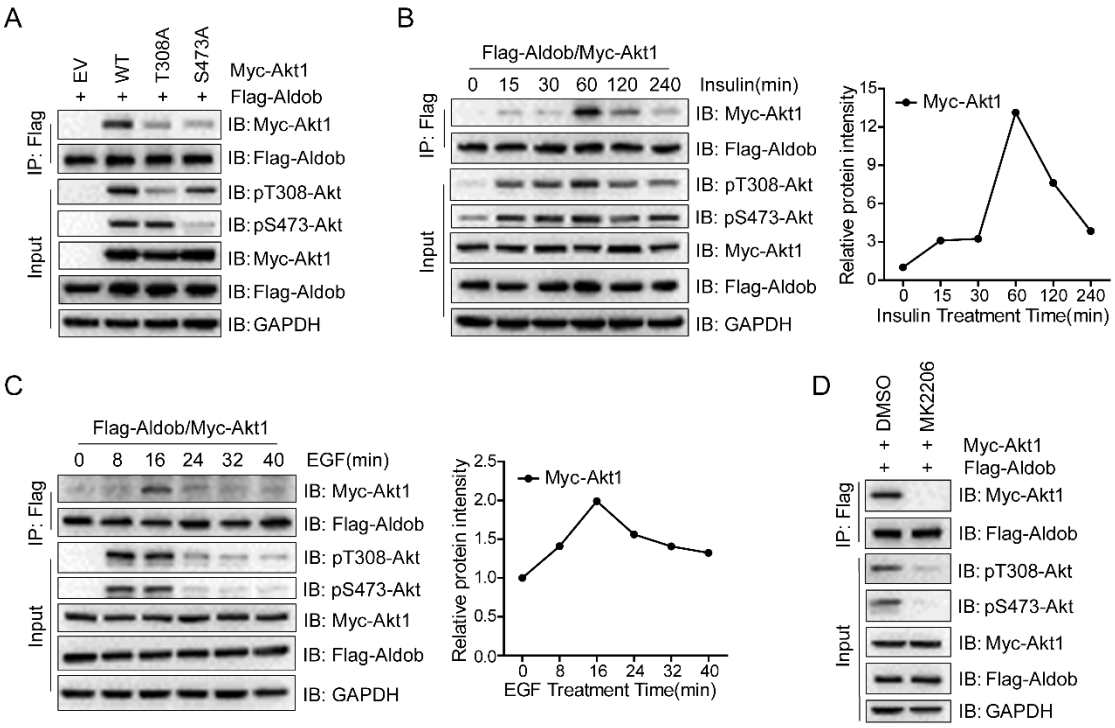

Fig 5. Aldob preferentially interacts with the phosphorylated species of Akt1.

(A) IB analysis of anti-Flag IP and WCL derived from Huh7 cells transfected with the indicated constructs. T308A and S473A indicated that threonine at position 308 and serine at position 473 of Akt1 were replaced by alanine, respectively. **(B** and **C)** IB analysis of anti-Flag IP and WCL derived from Huh7 cells transfected with Flag-Aldob and Myc-Akt1. Resulting cells were serum-starved for 24 hours and then stimulated with 0.1 μM insulin **(B)** or 100 ng/ml EGF **(C)**. At the indicated time points, WCL were harvested for Flag-IP and further for IB analysis (left). The relative intensity of Myc-Akt1 immunoprecipitated by Flag-Aldob was quantified (right). **(D)** IB analysis of anti-Flag IP and WCL derived from Flag-Aldob and Myc-Akt1 transfected Huh7 cells that were treated with DMSO or MK2206 (1 μM) for 24 hours before harvesting.

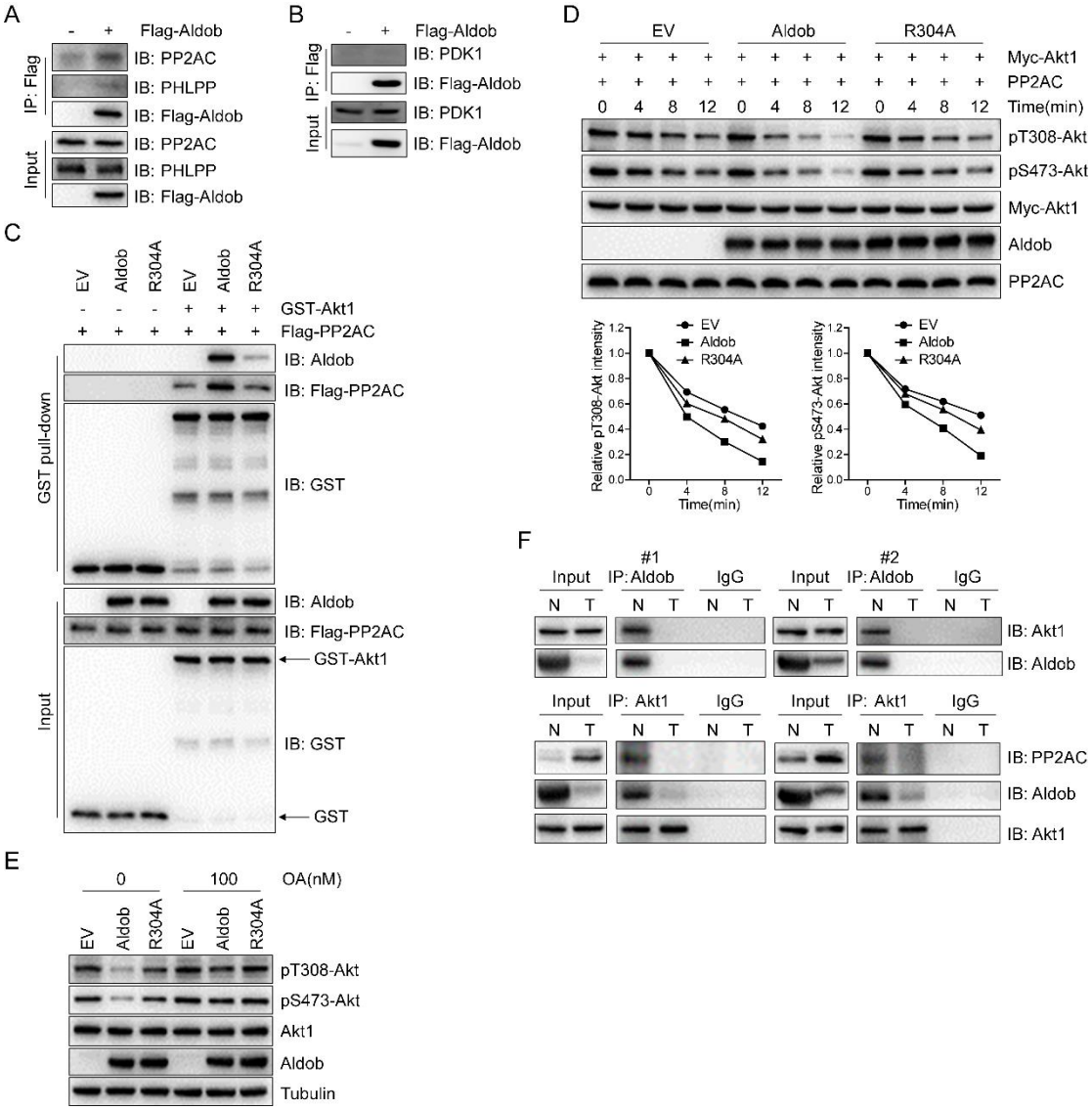

Fig 6. Aldob regulates Akt activity through protein phosphatase PP2A.

(A and **B)** IB analysis of anti-Flag IP and WCL derived from Huh7 cells transfected with the indicated constructs. **(C)** GST pull-down assays were performed with WCL derived from Flag-PP2AC transfected Huh7 cells and recombinant proteins GST-Akt1 and WT-Aldob or Aldob-R304A mutant. GST was used as the negative control. **(D)** *In vitro* PP2A dephosphorylation assays were performed with phosphorylated Myc-Akt1 and active PP2A in the presence or absence of recombinant WT-Aldob or Aldob-R304A mutant (top). The relative signal intensities of pT308-Akt and pS473-Akt were quantified (bottom). **(E)** IB analysis of WCL derived from Huh7 cells transfected with the indicated constructs. Resulting cells were treated 4 hours with okadaic acid (OA) at 100 nM. **(F)** IB analysis of endogenous anti-Aldob and anti-Akt1 IP and WCL derived from 2 pairs of human HCC samples. IgG was used as the negative control.

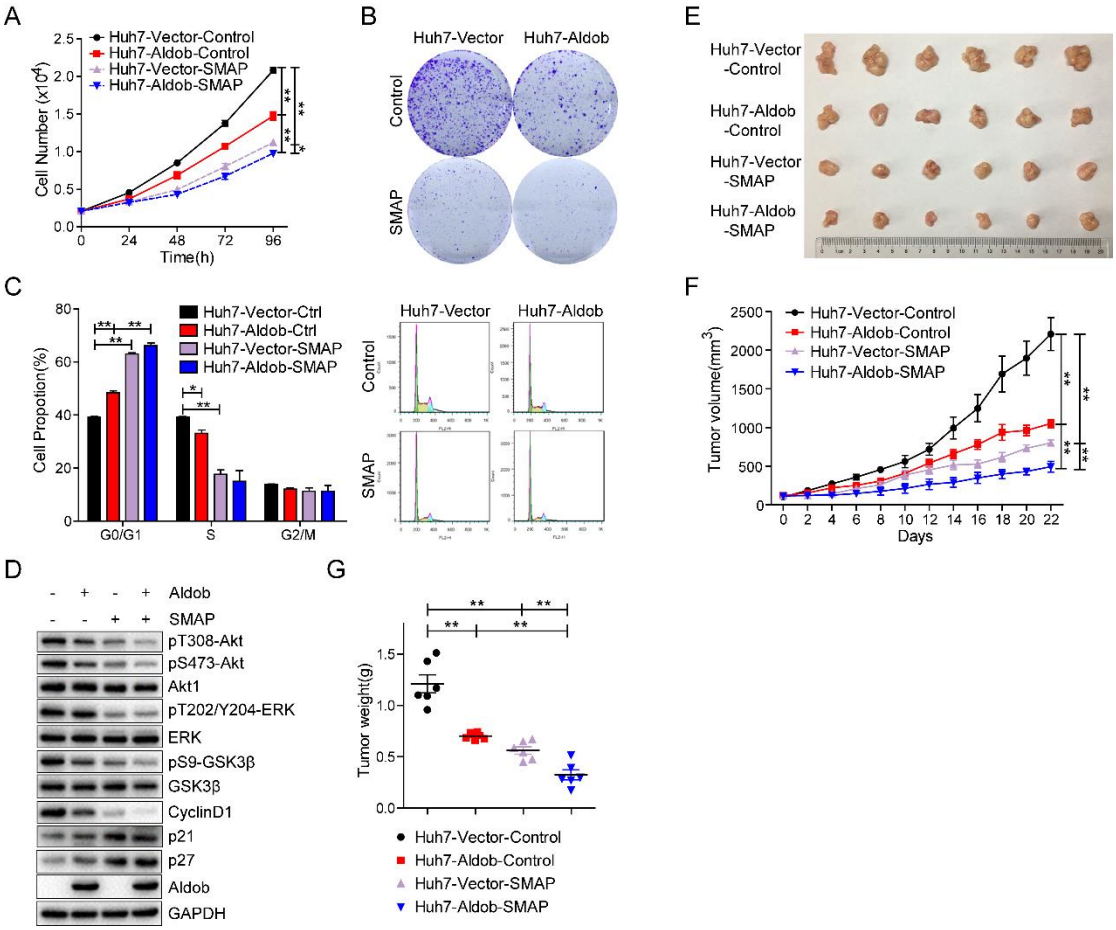

Fig 7. Activation of PP2A with SMAP potentiates Aldob-mediated tumor-suppressive role.

(A) Cell proliferation of Huh7-Vector and Huh7-Aldob cells in the presence of DMSO or SMAP (10 μM). **(B)** Representative graphs from colony formation assay of Huh7-Vector and Huh7-Aldob cells after exposure to DMSO or SMAP (10 μM) for 14 days. **(C)** Huh7-Vector and Huh7-Aldob cells were treated with 10 μM SMAP for 24 hours and cell cycle distribution was monitored by FACS. **(D)** IB analysis of WCL derived from Huh7-Vector and Huh7-Aldob cells treated 20 hours with control DMSO or SMAP (10 μM). **(E-G)** Representative tumor images **(E)**, xenograft tumor volume **(F)** and tumor weight **(G)** of Huh7-Vector and Huh7-Aldob xenograft tumors from control solvent and SMAP-treated nude mice (n=6 mice). Data are presented as mean ± SEM. * $p < 0.05$; ** $p < 0.01$ (Student's t-test).

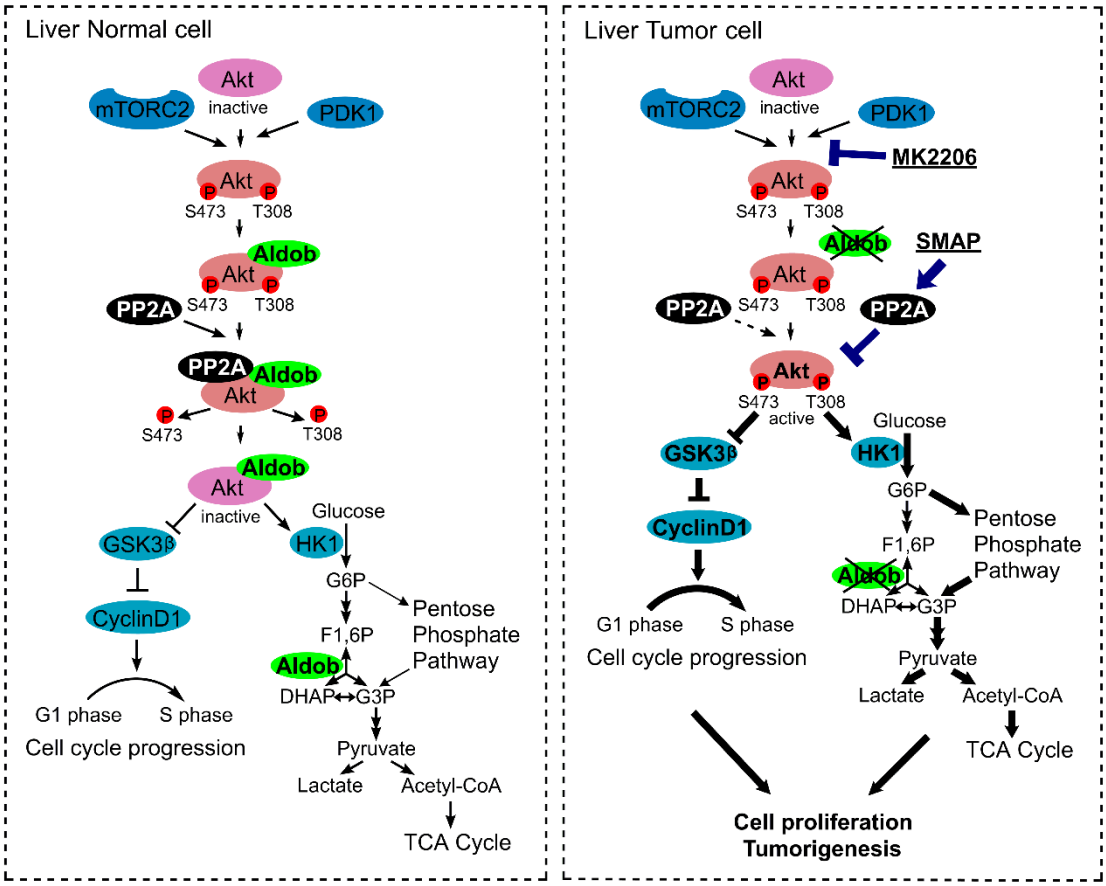

Fig 8. A schematic model of Aldob-mediated negative regulation of Akt activation. In normal cells, Aldob interacts with Akt in an Akt kinase activity-dependent manner, which promotes phosphatase PP2A binding to p-Akt and results in p-Akt dephosphorylation. Aldob is involved in the intracellular homeostasis of Akt phosphorylation through modulating substrate/phosphatase interactions. In Aldob-deficient cancer cells, downregulation of Aldob releases its negative regulation of Akt activity, leading to constitutive activation of oncogenic Akt signaling which facilitates cell cycle progression and increases metabolic flux to glycolysis and TCA cycle for cancer cell proliferation and tumorigenesis. Targeting hyperactive Akt through directly inhibiting Akt activity or reactivating PP2A phosphatase activity may be a viable therapeutic approach to treat Aldob-deficient human cancers. Bold arrows represent up-regulation of indicated signaling events in response to the absence of Aldob.

Supporting information

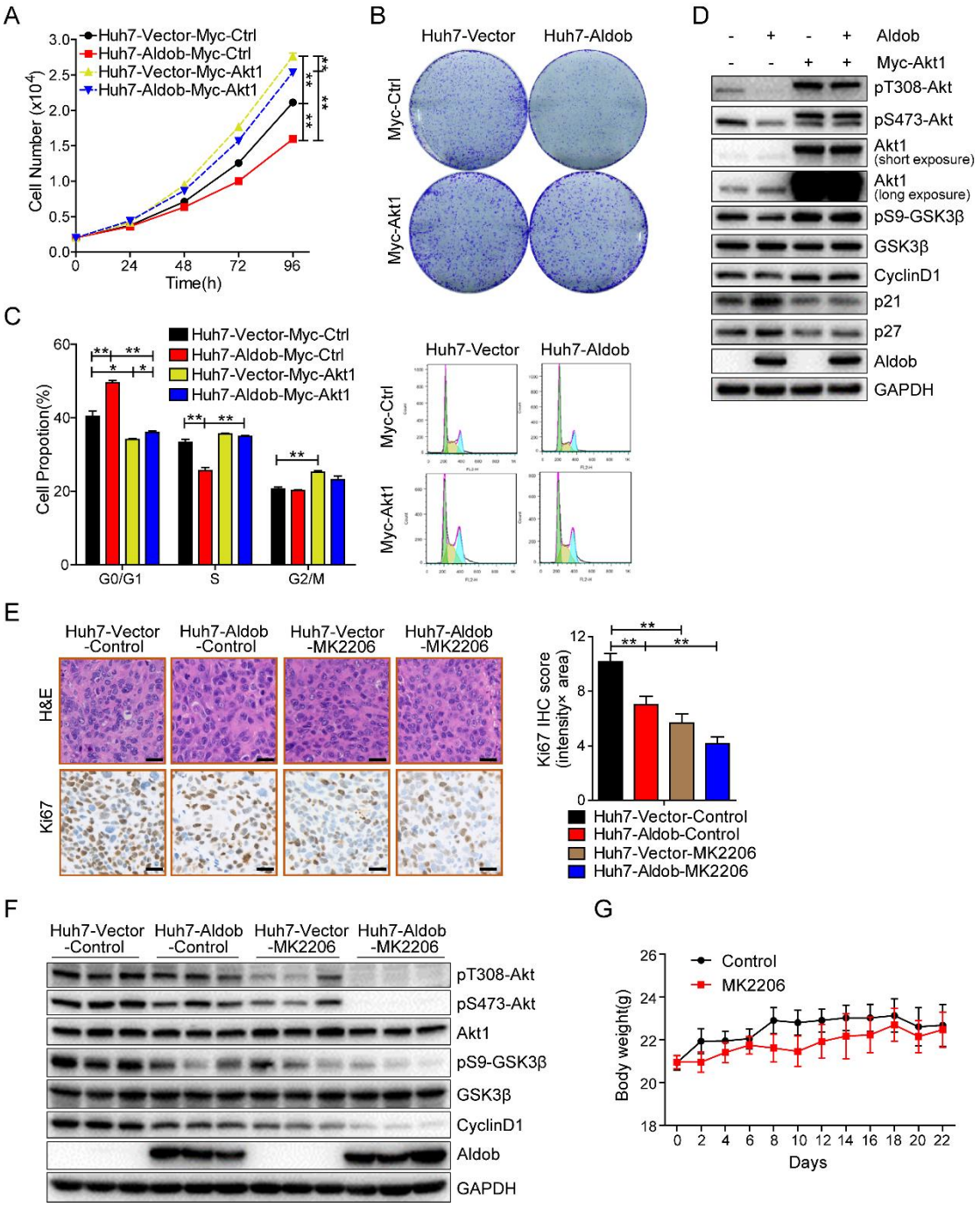

S1 Fig. Forced expression of Akt in Aldob-overexpressing cells eliminates Aldob-mediated tumor-suppressive effects.

(A) Cell viability assay of Huh7-Vector and Huh7-Aldob cells transfected with Myc-Ctrl or Myc-Akt1 constructs. **(B)** Representative graphs from colony formation assay of Huh7-Vector and Huh7-Aldob cells after transfection with Myc-Ctrl or Myc-Akt1 for 7 days. **(C** and **D)** Cells were transfected with Myc-Ctrl or Myc-Akt1 for 48 hours, and then monitored for cell cycle distribution **(C)** or subjected to IB analysis **(D)**. **(E)**

Representative IHC images and quantification of Ki67 expression in Huh7-Vector and Huh7-Aldob xenograft tumors treated with control solvent or MK2206 (n=6). Scale bars, 50 μm. **(F)** IB analysis of WCL derived from Huh7-Vector and Huh7-Aldob tumors treated with control solvent or MK2206. **(G)** The body weights of mice in Fig 3H were recorded. Data are presented as mean ± SEM. * $p < 0.05$; ** $p < 0.01$ (Student's t-test).

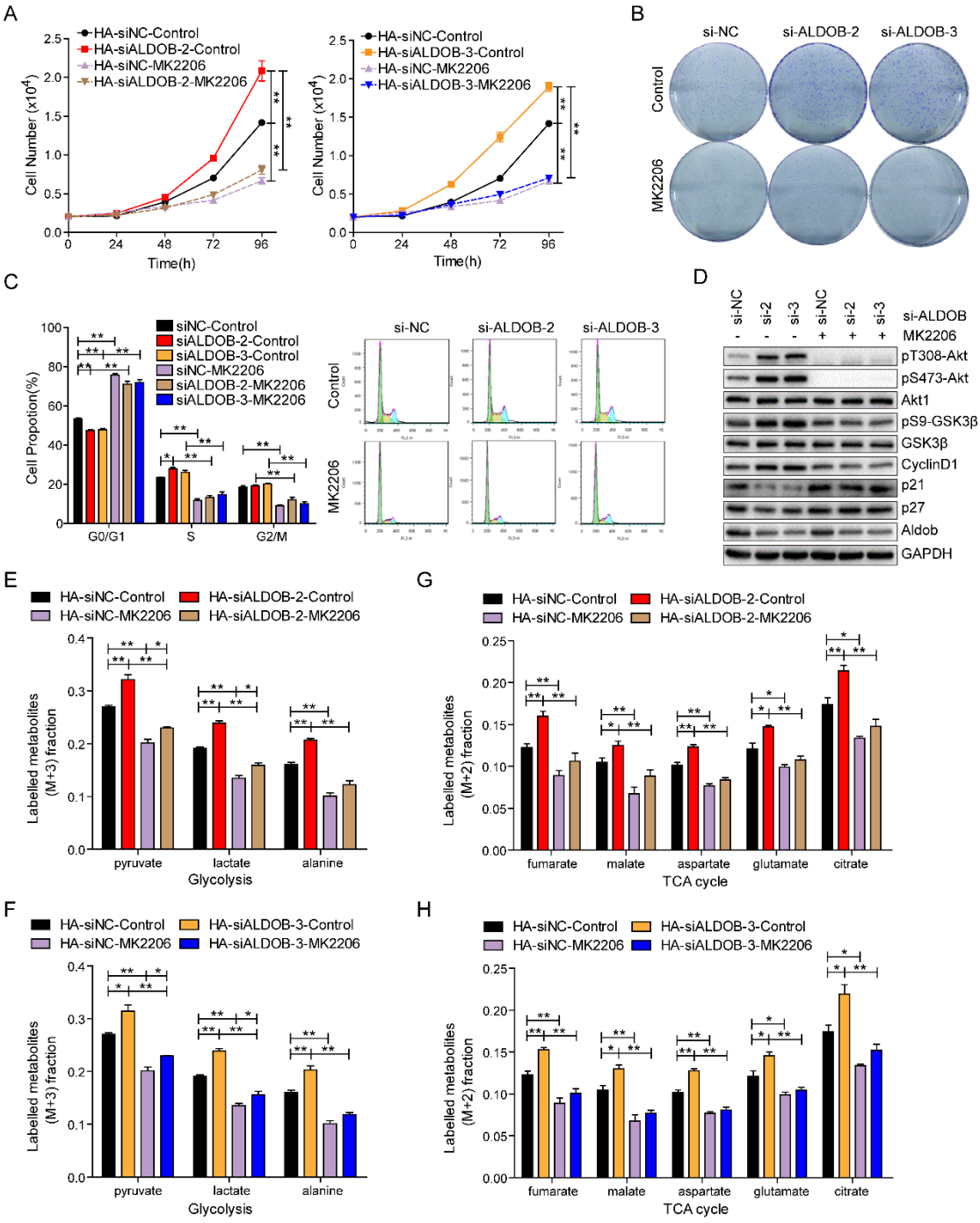

S2 Fig. Inhibition of Akt kinase activity is essential for Aldob-induced anti-tumor effects.

(A-D) Aldob-overexpressing Huh7 cells transfected with indicated siRNAs were used to determine their effects with or without MK2206 treatment (2 μM) on cell proliferation **(A)**, colony formation **(B)**, cell cycle distribution **(C)** and cell cycle-related protein levels **(D)**. **(E** and **F)** Fraction of the labeled metabolites of M+3 from ^{13}C-glucose in glycolysis by DMSO or MK2206 (5 μM) treatment for 12 hours in Huh7-

Aldob cells transfected with indicated siRNAs. (**G** and **H**) Fraction of the labeled metabolites of M+2 from ^{13}C-glucose in TCA cycle by DMSO or MK2206 (5 μM) treatment for 12 hours in Huh7-Aldob cells transfected with indicated siRNAs. Data are presented as mean ± SEM. * $p < 0.05$; ** $p < 0.01$ (Student's t-test).

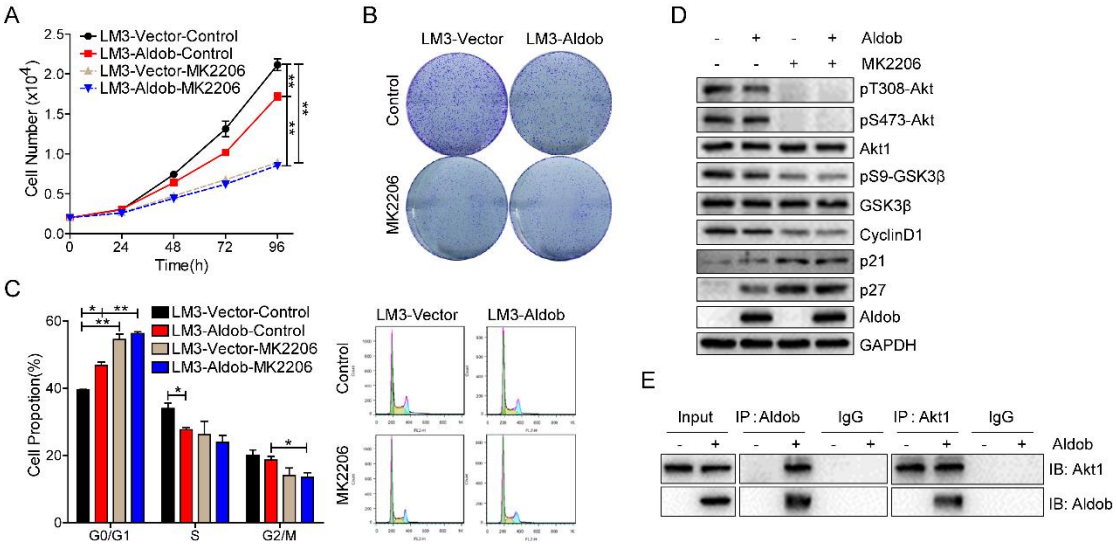

S3 Fig. Aldob inhibits HCC cell growth through suppression of Akt signaling.

(A-D) LM3 cells stably expressing Aldob via lentiviral infection (with Vector as a negative control) were used to examine their biological functions in the presence of either control DMSO or MK2206 (2 μM), including cell proliferation **(A)**, colony formation **(B)**, cell cycle distribution **(C)** and the protein levels of Akt pathway **(D)**. **(E)** Co-IP analysis to demonstrate the interaction between exogenous Aldob and endogenous Akt1 in LM3-Aldob cells. Data are presented as mean ± SEM. * $p < 0.05$; ** $p < 0.01$ (Student's t-test).

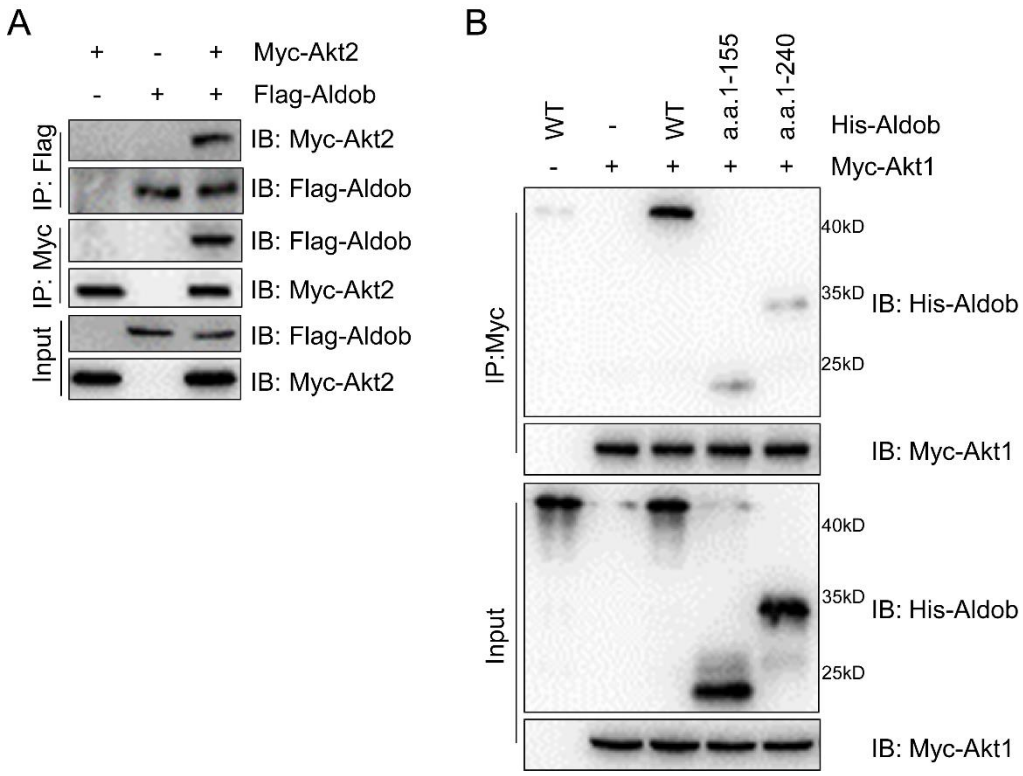

S4 Fig. Aldob directly interacts with Akt to inhibit Akt activity.

(A) Co-IP assay to show that Akt2 interacted with Aldob in Huh7 cells at ectopic expression conditions. **(B)** IP analysis was performed with WCL derived from Myc-Akt1 transfected Huh7 cells and various truncated mutants of recombinant His-Aldob proteins to illustrate that the C-terminal region (a.a. 241-364) of Aldob is responsible for Akt1-binding.

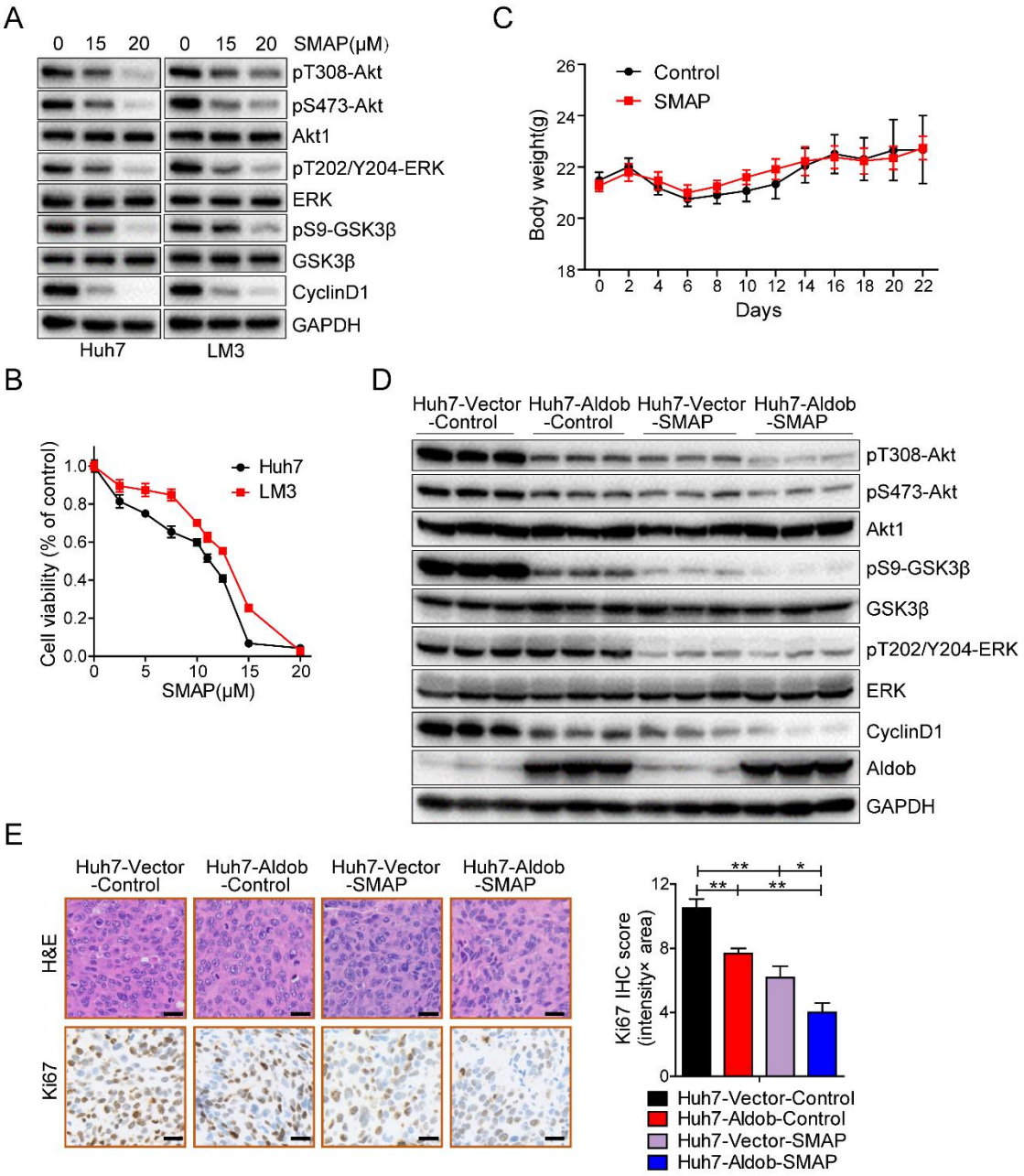

S5 Fig. PP2A activation with SMAP reduces Akt phosphorylation and suppresses HCC cell growth.

(A) IB analysis of WCL derived from Huh7 and LM3 cells treated with SMAP for 24 hours at the indicated concentrations. **(B)** Relative cell viability of Huh7 and LM3 cells treated with increasing concentrations of SMAP for 48 hours. **(C)** The body weights of mice in Fig 7E were recorded. **(D)** IB analysis of WCL derived from Huh7-Vector and Huh7-Aldob tumors treated with control solvent or SMAP. **(E)** Representative IHC images and quantification of Ki67 expression in Huh7-Vector and Huh7-Aldob xenografts treated with control solvent or SMAP (n=6). Scale bars, 50 μm. Data are presented as mean ± SEM. * $p < 0.05$; ** $p < 0.01$ (Student's t-test).

S1 Table. Association of clinicopathological characteristics with Aldob and p-Akt expression in HCC patients (n=70).

Variable	Aldob (total n=70)			pT308-Akt (total n=70)		
	Low expression (n=34)	High expression (n=36)	p	Low expression (n=38)	High expression (n=32)	p
Background						
Male	32 (94.1%)	35 (97.2%)	.522	37 (97.4%)	30 (93.8%)	.456
Age (y)	46.0 ± 8.4	47.0 ± 10.0	.652	46.0 ± 9.5	47.1 ± 9.0	.161
HBsAg	33 (97.1%)	34 (94.4%)	.589	37 (97.4%)	30 (93.8%)	.456
HBeAg	15 (44.1%)	11 (30.6%)	.241	14 (36.8%)	12 (37.5%)	.955
Anti-HBcAg	33 (97.1%)	35 (97.2%)	.967	36 (94.7%)	32 (100.0%)	.188
HBV-DNA ($\times 10^4$/mL)	15.5 (0.0, 32000.0)	12.5 (0.0, 2500.0)	.199	14.0 (0.0, 3200.0)	11.5 (0.0, 1400.0)	.478
Liver cirrhosis	34 (100.0%)	35 (97.2%)	.328	37 (97.4%)	32 (100.0%)	.355
AFP (ng/mL)	1067.4 (1.8, 1210.0)	54.2 (2.0, 1210.0)	.000*	230.8 (1.8, 1210.0)	292.7 (2.7, 1210.0)	.580
Liver function						
ALT (IU/L)	42.5 (18.0, 145.0)	41.0 (17.0, 320.0)	.370	42.5 (19.0, 320.0)	39.5 (17.0, 83.0)	.203
AST (IU/L)	42.5 (19.0, 160.0)	35.5 (20.0, 172.0)	.452	39.5 (19.0, 172.0)	40.5 (20.0, 120.0)	.326
Total bilirubin (μmol/L)	13.4 (5.3, 626.5)	12.2 (5.4, 384.1)	.961	12.3 (5.3, 626.5)	14.6 (6.4, 384.1)	.651
Albumin (g/L)	41.3 (34.6, 49.3)	43.0 (37.1, 53.4)	.036*	41.2 (34.6, 53.4)	42.8 (34.9, 49.8)	.356
PT (s)	12.1 (10.8, 15.3)	12.1 (10.4, 15.3)	.156	12.3 (11.0, 15.3)	11.8 (10.4, 13.3)	.001*
Tumor Factors						
Tumor size (cm)	7.5 (1.0, 17.0)	6.0 (2.0, 13.0)	.166	6.0 (1.0, 17.0)	7.5 (2.0, 15.0)	.507
No. tumor	29 (85.3%)	32 (88.9%)	.579	37 (94.7%)	25 (78.1%)	.039*
Macro-vascular invasion	4 (11.8%)	6 (16.7%)	.558	5 (13.2%)	5 (15.6%)	.769
Pathologic factors						
Tumor capsule	7 (20.6%)	12 (61.1%)	.001*	20 (52.6%)	9 (28.1%)	.038*
Micro-vascular invasion	18 (52.9%)	12 (33.3%)	.098	17 (44.7%)	13 (40.6%)	.729
Differentiation (III)	29 (85.3%)	24 (66.7%)	.069	28 (73.7%)	25 (78.1%)	.666
Recurrence (month)	6.7 (1.0, 35.0)	15.8 (1.0, 35.6)	.038*	15.1 (1.0, 35.6)	5.7 (1.0, 35.2)	.236
Overall survival (month)	20.8 (1.3, 35.6)	26.7 (5.1, 36.3)	.016*	25.7 (5.1, 36.3)	19.8 (1.3, 35.2)	.029*

AFP: Alpha-fetoprotein. ALT: Alanine aminotransferase. AST: Aspartate aminotransferase. PT: Prothrombin time. Aldob and p-Akt expression were defined as staining intensity. Protein expression intensity was classified into negative, weak, moderate, strong. The score calculation formula: (weak + moderate + strong)/ (negative + weak + moderate + strong) × 100%. Aldob and p-Akt expression score >50% are high, expression score <50% are low. * $p < 0.05$ by $\chi 2$ test.